© Copyright 2019

Sifang Chen

Building Programmable Matter Through DNA-based Chemical Computing

Sifang Chen

A dissertation

submitted in partial fulfillment of the

requirements for the degree of

Doctor of Philosophy

University of Washington

2019

Reading Committee:

Georg Seelig, Chair

James Carothers

Paul Wiggins

Program Authorized to Offer Degree:

Department of Physics

University of Washington

Abstract

Building Programmable Matter Through DNA-based Chemical Computing

Sifang Chen

Chair of the Supervisory Committee:

Associate Professor Georg Seelig

Electrical Engineering and Computer Science & Engineering

Biology offers compelling proof that macroscopic "living materials" can emerge from reactions between diffusing biomolecules. This work presents how molecular self-organization could be a similarly powerful approach for engineering functional synthetic materials. We focus on programmable DNA-hydrogels that produces tunable patterns at the centimeter length scale. We generate these patterns by implementing chemical reaction networks through synthetic DNA complexes, embedding the complexes in hydrogel, and triggering with locally applied input DNA strands. Chapter 1 provides an overview of the state of the art in programmable matter research. It also examines where current approaches, such as modular robotics and nanoscale engineering, may fall short. Chapter 2 presents chemical reaction-diffusion as an alternative approach to synthesizing programmable materials. Chapter 3 describes DNA computing and why it is ideal for realizing programmable reaction-diffusion systems. Chapters 4 and 5 introduce the DNA-based

reaction-diffusion systems we have implemented for making programmable spatial patterns. In Chapter 4, we demonstrate a DNA-based multi-layered cascade circuit where each layer consists of signal generation, signal suppression, and signal restoration modules. In Chapter 5, we couple *in vitro* experiments with computer simulation to demonstrate programmable spatial patterns that can be designed and simulated in advance.

ACKNOWLEDGEMENTS

This work would not be possible without the support from the incredible mentors, friends, and colleagues that surrounded me over the last six years.

My growth as a scientist owes a great deal to my advisor and colleagues at the Seelig Lab. Joining the Seelig Lab had been a significant shift in research direction for me – from experimental physics to DNA nanotechnology. Yet Georg entrusted me with an unusual amount of freedom to pursue my own research interest. This trust gave me the confidence to explore research ideas without the fear of failure and encouraged me to learn from mistakes. His emphasis on scientific rigor and clear communication pushed me to become a more systematic thinker, and become better at analyzing and articulating my research. Throughout, Georg has been an enthusiastic supporter of my ideas and career choices, even when those ideas are sometimes literally out of this world.

I've also been lucky to be surrounded by a group of fantastically brilliant, kind, and fun labmates. It was refreshing to be in the midst of such diverse technical and cultural perspectives. I learned the fundamentals of DNA nanotechnology by siphoning from the combined wisdoms of Sherry Chen, Yuan-jyue Chen, and Gourab Chatterjee. In yet another testament to the interdisciplinary nature of our lab - Yuan (an electrical engineer by training) taught me Pipette 101. I want to thank Alex Rosenberg for being a great friend, who can always be counted on to instigate adventures. I want to thank Ben Groves and Nick Bogard, for their many failed and hilarious attempts to instill cynicism and skepticism in me. I also want to thank Sumit Mukerjee, Johannes Linder, Charles Roco, and Alberto Carigioni for all the stimulating and eye-opening conversations over the years.

I have found lifelong friends in Randolph Lopez, Sunny Rao, Chuhern Hwang, and Ahmed Qureshi. It’s impossible to distill our friendships in so few words. Whether it's scaling mountain tops or working into the wee hours of night, putting on musicals or campaigning for political candidates, they are my constant support as well as catalysts nudging me to step out of my comfort zone. I also owe my thanks to Lee Organick and Sarah Harrison, who are the most kind and badass roommates one can ask for.

It's always been important for me to apply what I've learned toward real world solutions. Today, we're faced with unprecedented challenges and opportunities because of climate change. I'm grateful for the chance to work alongside Bichlien Nugyen and Asta Roseway, and apply my knowledge to help solve environmental challenges.

I wouldn't be here without my undergraduate advisors Joshua Folk and Rogerio de Sousa, who have been instrumental in fostering my interest in research. Working in their labs helped me build a solid foundation as a budding scientist.

I want to thank my partner Ayah, for their constant support and for inspiring me to be my best self. I'm grateful to my parents for my educational opportunities, even when it meant putting their own careers on hold. This thesis is dedicated to the memory of my grandfather, whose compassion and strength of character will always be an inspiration.

Table of Contents

Chapter 1 Programmable materials

1.1 Background

The notion of "intelligent matter" has long captured the human imagination – objects that take up new functions and appearances on command are a fixture in many of our most enduring science fiction and fantasy stories. Today, active research is being directed toward bringing this idea to reality. Specifically, programmable matter research - an emerging field that leverages advances in electronics, nano- and biotechnology - aims to engineer materials that can undergo physical transformations when triggered by environmental stimuli or user-define inputs. Programmable materials research is attracting growing interest because it could enable paradigm shifts in multiple industries. Figure 1 shows a selection of applications under active research. For example, we could weave thermal-regulating clothes from heat-adaptive fabrics[1], assemble buildings from modular construction units, manufacture lighter and stronger aircraft wings from programmable composite materials[2], and reduce waste by using shape-morphing and multi-functional objects.

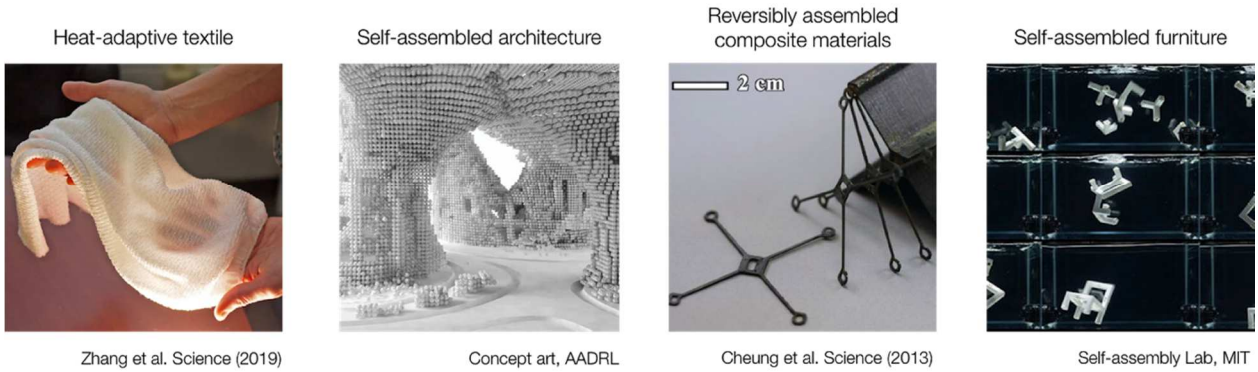

Figure 1. Emerging applications of programmable materials. Programmable materials can be used to **a)** make novel textiles; **b)** develop self-assembling buildings; **c)** manufacture adaptive construction materials; **d)** make shape-morphing everyday items.

Moreover, we can expect programmable materials to have profound implications on how we perceive and interact with the physical world. The potential applications are only limited by the bounds of our imagination.

1.2 Current approaches

Current approaches to constructing programmable materials fall into two categories: 1) coordinating multiple intelligent agents to carry out information processing; 2) embedding programmability directly into the material via advanced materials synthesis. This section provides a brief overview of these approaches and identifies where they fall short. The relevant systems are described in order of the construct size (meter → centimeter → nanometer).

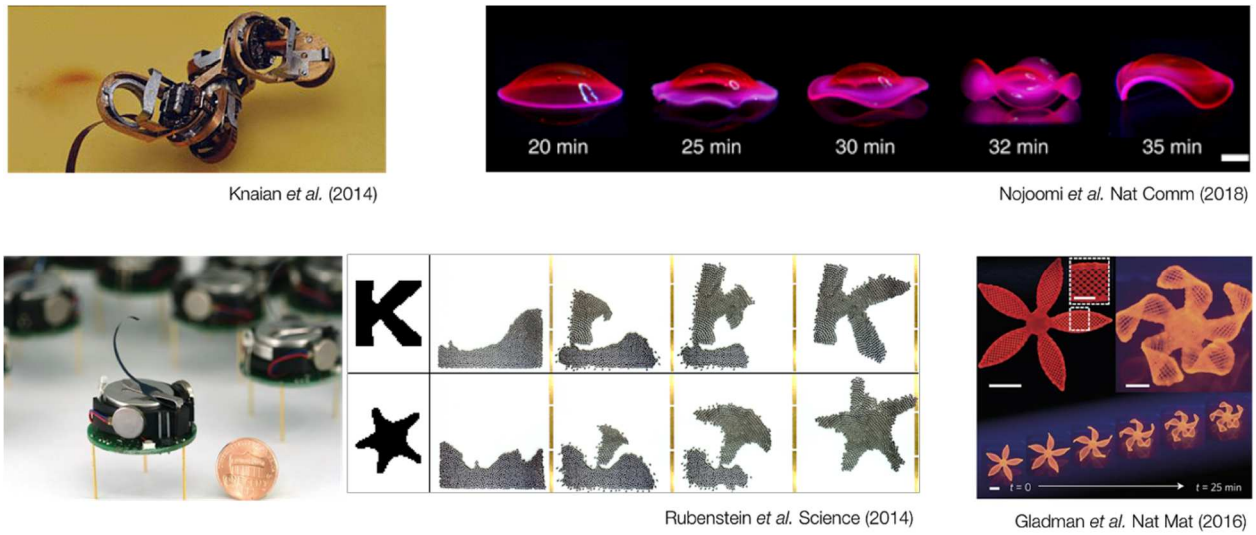

Figure 2. Current research approaches to building programmable matter. Top left: a snake-like robot consisting of 1 cm long linkers that can rotate independently. **Bottom left:** systems of one thousand modular robots that can self-organize into programmed shapes. **Top right**: hydrogel crosslinked in precise locations such that it can reversibly transform into different configurations when sensing temperature changes. **Bottom right:** 3D printed flower using a special polymer such that it changes shape when submerged in water.

Meter-scale constructs

Modular robotic systems are popular for building dynamic structures at the macroscopic scale. Researchers have demonstrated fleets of modular robots that coordinate to form self-organized (2D) structures, emulating the swarm behavior commonly exhibited by birds and insects[3]. Typically, each robotic unit contains microcontrollers for signal processing, motors for maneuvering into desired positions, and sensors for detecting and avoiding nearby objects. In systems aimed at constructing cohesive structures, the units are also outfitted with permanent or temporary physical linkers.

Modular robotic systems have the advantage of being highly programmable, but their reliance on electronic parts imposes an inherent limit on their size and flexibility. At the minimum, each unit needs transceivers, actuators, batteries, micro controller, and a chassis. As such, the smallest modular robots are still on the order of a centimeter[4]. In self-assembling systems, depending on the docking mechanism, connections between units are either weak or power intensive[5,6], which are undesirable for building robust programmable matter. Further, ensuring reliable communication between subunits remains a formidable challenge in distributed computing. All these constraints make it difficult to produce more adaptive and scalable systems.

Centimeter-scale constructs

Advances in additive manufacturing have begun to bridge the gap between macro- and micro-structures. As 3D printing matures, we have seen vast improvements in the resolution, complexity, and material versatility of 3D printed constructs. First, higher resolution and precision enable the design and construction of smaller and more intricate parts. As this trend continues, 3D printing

may one day become precise enough to build mesoscopic structures. Second, 3D printing allows for unprecedented design complexities. For example, engineers can now control the thickness of different printed parts and fine tune their flexibility[7]. These techniques have been used to build structures capable of transitioning between different configurations in response to heat[8], stress[8–10] or moisture[7,11,12]. Third, 3D printing can combine multiple materials within the same structure. These materials can be interwoven in well-defined ways to add extra layers of programmability into the resulting structure[13].

Using novel synthesis methods, researchers have also developed functional materials that display interesting colorimetric or conformational changes when exposed to stress[14] or heat gradients[15–17]. Figure 2 shows one such hydrogel-based material that has been cross-linked in certain areas such it can shapeshift when experiencing temperature changes.

Constructs made with these methods have embedded programmability. However, compared to robotic systems, they are more limited in their information processing capacity and the range of compatible input signals.

Nano-scale constructs

Eric Drexler conceived constructing programming matter via the massive scaling up of molecular manufacturing. In his vision, synthetic molecules would form the basis of dynamic macroscopic structures called utility fogs[18]. Because each molecule would in principle be controlled independently, utility fogs would possess much finer resolutions for control and movement, and can form any number of structures on command. The pursuit of such visions has led to remarkable

progress in engineering atomic and molecular machines that operate at the nanometer scale. Scientists have used photo- and electron-lithography to fabricate miniature mechanical parts like gears and rotors, which can be actuated via electrical[19] or optical signaling[20]. However, these individual parts still lack the means to communicate, coordinate, and form into larger structures. Further, creating components through nanofabrication is extremely resource intensive, and therefore impractical for building structures beyond the mesoscopic length scale.

Creating "materials that compute" is the grand challenge of programmable matter research. As this brief overview shows, existing engineering approaches are each faced with imposing technical hurdles: modular robotic systems are constrained by the size of their components; advanced materials and metamaterials have limited functionality; methods for scaling up molecular manufacturing remain out of sight. Are there alternative approaches to overcome these hurdles? As usual, we can turn to nature for inspiration.

1.3 Programmable materials in nature

Living organisms are exceptional at sensing and responding to changes in their environment, using endogenous mechanisms for processing biological, chemical, and optical signals.

In fact, biological pattern formation is ubiquitous. From camouflage, to chemotaxis and morphogenesis, biology displays self-organization and self-assembly at all length scales. The existence of such dynamic patterns and structures suggests that complex and environmentally responsive systems could arise from the self-organization of information-bearing agents like molecules or cells.

As synthetic biologists, we are bound to ask: how can we re-engineer and repurpose organisms to perform functions that we care about? We can extend this mindset to materials science as well: how can we build "living materials" that emulate the dynamic structure formation processes we see in biology? In biology, pattern formation, like all cellular processes, rely on networks of biochemical reactions.

Camouflage is used by several cephalopods to evade or ward off predators. When they sense danger, these cephalopods can camouflage by matching themselves to the color patterns of their environment. This is done via the contraction of chromatopohores, a special type of pigment cell in the skin of some cephalopods. Chromatophore contractions are coordinated by the nervous system and visual input from the cephalopods' well-developed eyes. Thus, camouflaging can occur within seconds of detecting a threat. Other marine animals like squids can produce bioluminescence using photophores and photocytes, which produce luciferase via the oxidation of luciferin. Species that have both photophores and chromatophores can control the size, color, and intensity of the pattern produced. During chemotaxis, organisms move along a chemical gradient either in search of food or to flee from toxins. Budrene et al. showed that complex, long-range spatial patterns could arise from E.coli chemotaxis[21]. They found that E.coli aggregate toward asparate, a chemical the bacteria excrete. In response to gradients of asparate, E.coli can form patterns of varying cell density. The patterns are found to vary in a systematic way depending on the initial conditions, such as the concentration of growth substrate succinate. For example, low concentrations of succinate resulted in a "single traveling band (swarm ring) that moves slowly outwards", while high concentrations of succinate resulted in "concentric rings in radial rows" and "intersecting spirals". The underlying mechanisms behind morphogenesis and animal coat

patterns still elude scientists today. We have yet to find a definitive answer to how cells organize into patterns like the stripes on zebras or spots on snow leopards. The most prominent theory was put forth by Alan Turing, who hypothesized that diffusing molecules interact to produce complex patterns. But today, experimental evidence show that the real mechanism may be more complicated than this. Yamanaka et al. showed that the yellow-and-black stripe pattern in zebrafish is the result of two types of cells engaged in a game of "run-and-chase"[22]. When yellow cells called xanthophore are close to black cells called melanophore, xanthophores will reach out to melanophores, which retreat in response, producing the stripe pattern. They also found that in mutant zebrafish, both types of cells have more subdued response. The yellow cells will chase less and the black cells will retreat less, resulting in a broader and fuzzier stripe pattern.

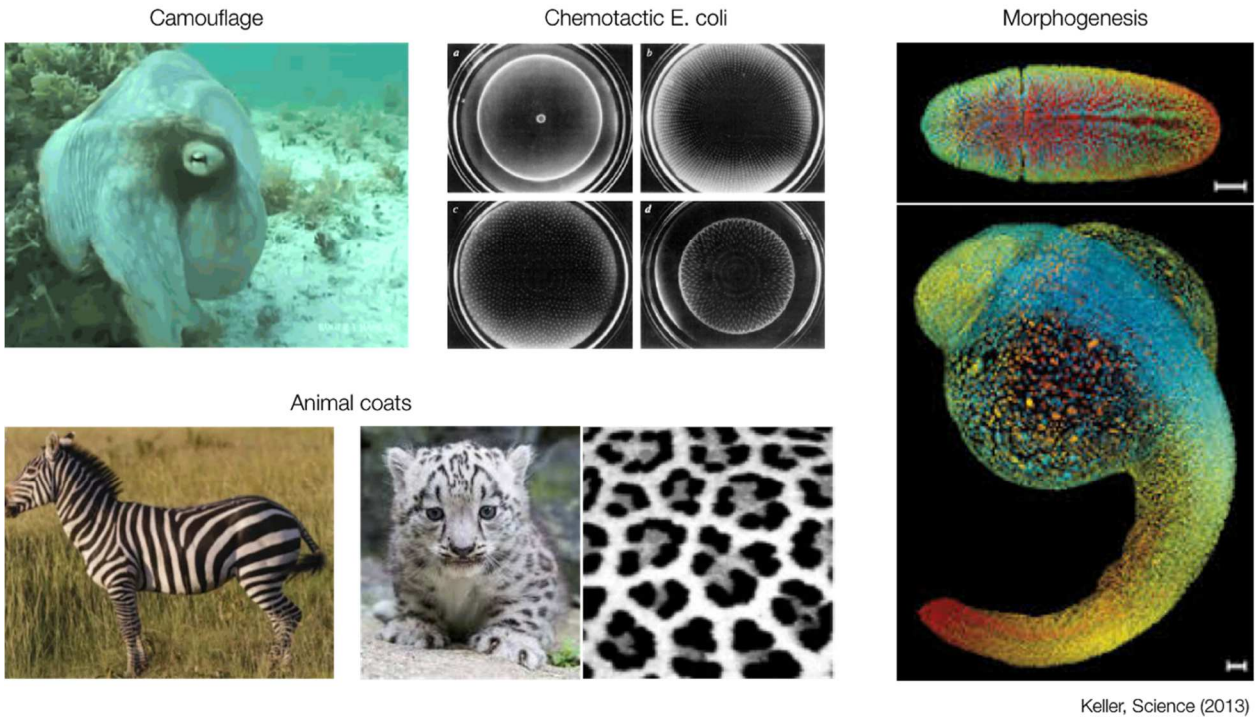

Figure 3. Dynamic pattern and structure formation in nature.

Chapter 2 Chemical computing

Digital and natural computing represent two paradigms for information processing. In digital computers, information is received, processed, and transmitted as electrical signals. By contrast, a chemical computer processes molecular signals. However, while digital computing is less than a hundred years old, chemical computers has been around for billions of years - life itself is a highly complex, energy-efficient, and chemically driven process. Even today, the efficiency and adaptability of living organisms remain unmatched by any man-made systems.

Biological organisms have developed sophisticated molecular machineries for processing chemical signals. These cellular processes depend on networks of chemical reactions to detect, process, and produce molecular inputs and outputs. Thus, chemical reactions are central to generating dynamic patterns and structures in biology. However, little attention has been directed toward engineering programmable materials using chemical computing. The lack of research effort in this area possibly derives from the difficulties in altering and controlling chemical reactions. To make programmable materials, engineers not only have to understand the system, but also have the means to tune the system within desired parameters. In the past, this has not been possible. We have thorough understanding of many chemical reactions, but programming chemical reactions has only become a reality in recent years.

2.1 Chemical computing in reaction-diffusion systems

This section examines how we can apply the principles of reaction-diffusion for chemical computing and engineering programmable materials. In reaction–diffusion systems, chemical

species transform into each other through reactions, and spread out in a medium through diffusion. Under the right conditions, a reaction-diffusion system could lead to the emergence of complex patterns.

Alan Turing first proposed reaction-diffusion to explain morphogenesis - the process of how organisms take shape[23]. In his landmark 1952 paper, The Chemical Basis of Morphogenesis, Turing postulated that morphogenesis arises from the "diffusion of two different chemical signals, one activating and one deactivating growth, to set up patterns of development". He dubbed these chemical signals "morphogens" - diffusive molecules that control cell differentiation by establishing concentration gradients. According to this model, patterns in nature, such as stripes and spots in animal coats and skin pigmentation, can emerge naturally out of a homogeneous state due to symmetry breaking caused by small localized perturbations in the concentrations of specific morphogens. As a result, reaction-diffusion systems have attracted much interest as a prototype model for pattern formation. Since then, other models have been proposed to explain biological pattern formation. Gierer and Meinhardt[24] argued that a system containing 1) slow moving activators and fast moving inhibitors and 2) autocalysis could produce self-organized patterns such as Turing patterns. Similarly, the Gray-Scott and Lotka-Voterra models propose alternative reactions for generating different patterns.

Much of the work done in reaction-diffusion spatial patterning has been computational. Satisfying the parameter constraints, such as the rate constants and diffusion coefficients of chemicals, has been a major obstacle in experimentally realizing Turing patterns. As a result, the number of in vitro patterning systems has remained disappointingly low.

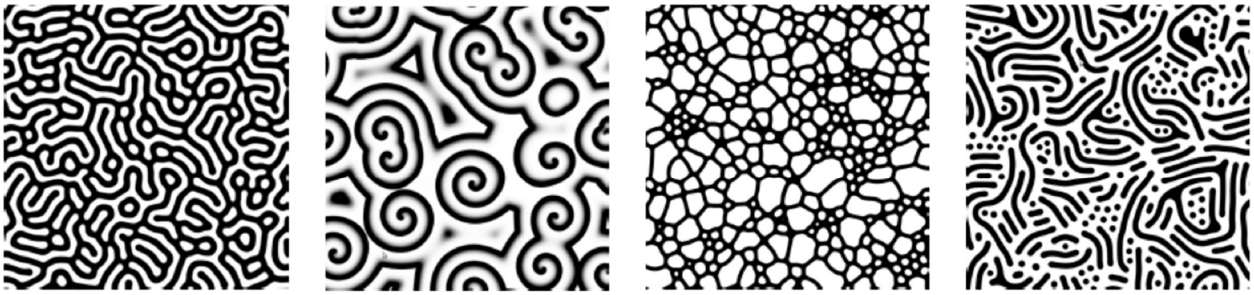

Figure 4 Simulations of reaction-diffusion patterns using the Gray-Scott model. Qualitatively different patterns can emerge by tuning reaction rate constants, diffusion coefficients, and initial morphogen concentrations.

2.2 Experimental realizations of reaction-diffusion systems

Pattern formation in synthetic chemistry

Since the 1960s, scientists have found many theoretical CRNs exhibiting interesting dynamics, including multiple steady states and oscillatory behaviors. One such example is the BZ reaction, which refers to a class of chemical reactions in which bromate ions oxidize an organic substrate in the presence of a transition metal ion. The first BZ reaction was discovered by the Soviet chemist Boris Belousov in 1950 while he was trying to develop a synthetic chemical system to model the Krebs cycle[25]. In his experiment, Belousov combined citric acid (organic substrate), cerium (transition metal), and bromate (oxidizing agent) in solution. Instead of the reaction proceeding to equilibrium and exhibiting a monotonic color transition as expected, Belousov observed the color of the reactor oscillating between yellow (oxidized state) and clear (reduced state). In general, the reaction is carried out in an acid solution, which acts as the organic substrate, with oxidation carried

out by bromate and transition metals. A reactor that uses ferroin as the transition metal can display a visible and compelling color transition from red to blue. Belousov and Zhabotinsky also found that carrying out the reaction in a spatial chemical reactor like a petri dish resulted in propagating waves and pattern formation, where the waves organize in patterns of concentric rings expanding away from the point of initiation. The BZ reaction is a prime example of a chemical oscillator and a far-from-equilibrium system, and can lead to chaotic and self-organizing behaviors. Because of this, the BZ reaction and other chemical oscillators have been of special interest to scientists studying non-equilibrium biological phenomena like Turing patterns. Non-equilibrium behaviors have been observed is in dielectric barrier discharge[26–28]. Here, a discharge cell is constructed by trapping gas in a thin layer between two planar electrodes. When a high voltage is passed between the electrodes, breakdown of the gaseous dielectric layer results in complex pattern formation like filaments, filament clusters, and concentric rings.

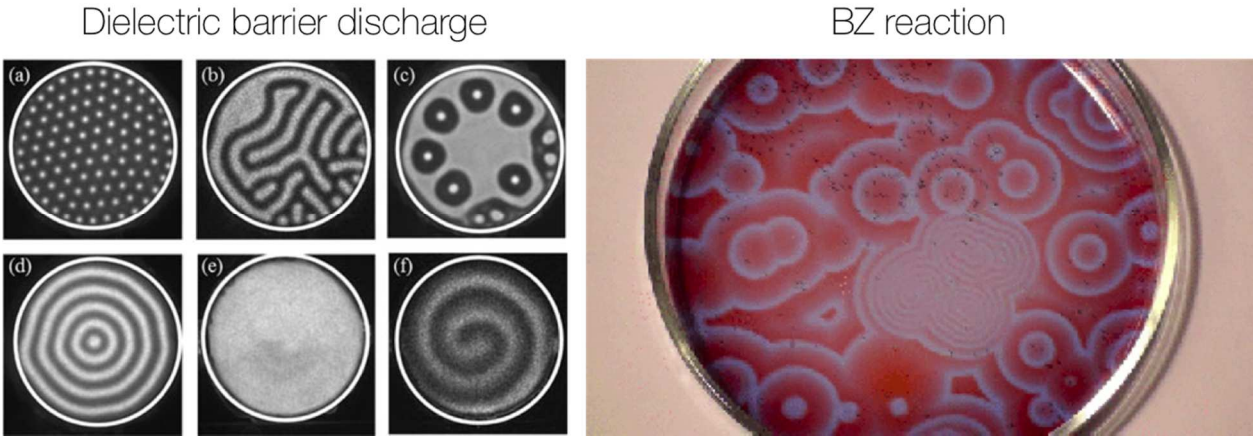

Figure 5 Pattern formation in physical and synthetic chemistry. Left: Pattern formations in dielectric barrier discharge. **Right:** Turing patterns in the BZ reaction, an example of a chemical oscillator.

Pattern formation in synthetic biology

The French flag model proposed by Lewis Wolpert provides an alternative explanation for pattern formation and morphogenesis[29]. Here, morphogen concentration gradients lead to a pattern containing three zones, much like the stripes on a French flag. Each zone corresponds to a chemically distinct state, and can turn "on" when the target morphogen has reached a specific threshold concentration. To create a French flag pattern, imagine a scenario where morphogen is fed into a rectangular reactor from the left side. Since the morphogen gradient decreases away from left edge due to diffusion, the left zone will turn "blue" under high morphogen concentration, the middle zone will turn "white" under medium morphogen concentration, and the right zone will turn "red" under low medium morphogen concentration.

The French flag model has served as an archetypal pattern for synthetic biologists building pattern forming systems. In their pioneering work, Basu et al. demonstrated stripe pattern formation by genetically engineering E. Coli, which were grouped into "senders" or "receivers"[30]. Sender cells produce AHL, which diffuses throughout the reactor. Receiver cells contain genetic circuits for detecting AHL concentration and fluoresce when the AHL concentration is within a user-define range. As a result, a bullseye pattern around the sender cells could emerge from an initially undifferentiated lawn of receiver cells. Liu et al. demonstrated periodic stripe patterns through bioengineered quorum sensing of E. coli[31]. They programmed the E. coli to have low motility at high cell densities by constructing a genetic circuit containing a density-sensing module and a motility-control module. This system was able to generate periodic stripe patterns autonomously. Further, the number of stripes could be tuned by modulating the basal expression of a single gene.

Synthetic quorum sensing systems have also been shown to enable basic pattern formation. Dupin et al. demonstrated pre-patterned synthetic multicellular compartments can communicate via small molecules to evolve toward desired final pattern[32]. Gines et al. showed microscopic beads dispersed in an enzymatic solution can perform distributed computing by emitting and processing chemical signals[33]. Such collective behavior led to coordinated formation of patterns.

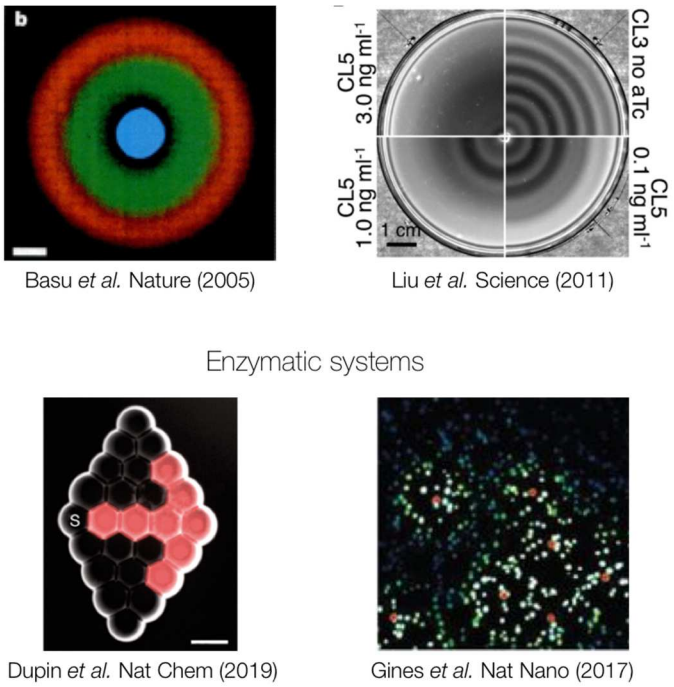

Figure 6 Pattern formation in biology. Top left: stripe pattern formation by genetically engineering E. Coli. **Top right:** periodic stripe patterns through bioengineered quorum sensing of E. coli. **Bottom left:** patterns developed from synthetic cellular compartments. **Bottom right:** microscopic beads dispersed in an enzymatic solution can perform distributed computing by emitting and processing chemical signals.

2.3 Chemical reaction networks

Chemical reaction networks (CRNs) are a convenient mathematical framework for studying the dynamics of real and abstract chemical systems. CRNs consist of a set of chemical reactions and

mutually interactive chemical species. The reactions are represented by chemical equations, according to the law of mass action. CRNs can be used to model how the concentrations of species evolve over time in a dynamic, non-equilibrium system.

A large body of theoretical work has been devoted to investigating dynamic behaviors in chemical reactors. Interest in computing with chemical reactions was spurred on by the discovery of the BZ reaction and other far-from-equilibrium-state chemical systems. In this context, a chemical circuit is composed of a set of chemicals that interact according to an algorithm (chemical reactions). Chemical computers are much slower compared to their digital counterparts. But chemistry has the advantage of massive parallelism and having the ability to interface with molecular signals. Further, researchers have demonstrated that CRNs are Turing Universal, meaning that they can compute anything that a von Neumann machine can.

It should be noted that even though CRNs have the potential to become a new computing paradigm, significant technical challenges remain. Implementing complex CRNs is nontrivial. Predicting and simulating CRN dynamics is often even more intractable. Most CRNs do not have analytical solutions and must be solved numerically. Finite element method (FEM) is a standard numerical approach to solving systems of differential equations. The theoretical basis for implementing FEM has been discussed at great length elsewhere and will not be elaborated here. Suffice to say that Visual DSD, the software we used for spatiotemporal modeling, employs FEM to simulate the dynamics of DNA-based reactions.

Chapter 3 DNA as a programmable material

DNA is well known for its role as carrier of biological information. But recent advances in DNA nanotechnology have demonstrated that synthetic DNA is a promising engineering material for building molecular circuits and nano-devices. Watson-Crick base pairing is highly precise and guarantees that complementary DNA sequences will always hybridize correctly. DNA nanotechnology exploits the precision of DNA base pairings to enable the rational design and construction of molecular systems for an ever-increasing array of applications. Researchers have designed DNA gates to implement dynamic, far-from-equilibrium CRNs to perform complex calculations and built 2D and 3D nano-structures using elementary DNA sequences. This section provides a brief overview dynamic and structural DNA nanotechnology.

3.1 DNA strand displacement

In DNA strand displacement, reactions are driven by the propensity for DNA molecules to minimize energy and maximize entropy. Unpaired bases have higher free energies than paired bases. Thus, DNA strands will tend to minimize the number of unpaired bases. During DNA strand displacement, two DNA complexes with partial or full complementarity interact with each other, displacing one or more pre-hybridized strands from the participating complexes. Consider a system containing two DNA species, A and B. Here, A is single stranded, while B is partially double stranded. The sequence of A is fully complementary to the bottom strand of B. The exposed sequence in B, called the toehold domain, will stochastically bind to A. The top strand in B, called the migration domain, will eventually be displaced by A through a random walk process. At chemical equilibrium, we will find A fully hybridized to the bottom strand of B, because this is

the state of minimum free energy. Zhang et al. conducted extensive study to characterize the thermodynamic properties of DNA strand displacement[34].

3.2 DNA computing using strand displacement

DNA strand displacement has been used to design and create numerous molecular systems with dynamic responses. Using only DNA strand displacement, Seelig et al. built Boolean logic gates with rationally designed synthetic DNA complexes as input and output signals[32]. The logic gates covered a complete set of logic functions (AND, NOT, and OR). They further implemented thresholding and amplification to increase the complexity of the circuit. Individual DNA-based logic gates need to be connected to build larger and more functional circuits. As such, feedback and signal amplification are important for connecting modules and preventing signal loss. Zhang et al. address this issue devising a design strategy that "allows a specified input oligonucleotide to catalyze the release of a specified output oligonucleotide, which in turn can serve as a catalyst for other reactions"[36]. Using their amplifying circuit element, they constructed feedforward cascade and positive feedback circuit showing exponential growth kinetics. Soloveichik et al. presented a systematic approach for approximating coupled chemical reactions (with unimolecular and bimolecular kinetics) using DNA strand displacement cascades[37]. Their methods showed that abstract chemical systems can be implemented with real chemical reactions. They simulated various chemical oscillators (Lotka-Volterra, limit-cycle, and chaotic system) using this method, laying the theoretical groundwork for using DNA strand displacement to implement complex CRNs. Qian et al. translated neural network nodes (Hopfield neurons) into strand displacement based logic gates[38]. They connected four such DNA-neurons and trained them in silico to remember a certain pattern. They then tested the artificial neurons in vitro by presenting them with

an incomplete pattern (in the form of DNA oligos), and showed that the neurons could recall the full pattern even when the input pattern was incomplete. Chen et al. developed an architecture for constructing DNA gates for performing chemical control within cells[39]. In contrast to logic circuits, their system can process analog biochemical input signals. Their method of deriving DNA gates from biologically synthesized plasmid greatly increased the fidelity of their DNA circuit, which enables the construction of larger and more complex systems.

3.3 Structural DNA nanotechnology

Structural DNA nanotechnology leverages the programmability of DNA to build 2D and 3D self-assembled constructs at the molecular length scale. The idea of using DNA as a structural engineering materials was first introduced by Nadrian Seeman. He showed that DNA sequences could be directed to form macromolecular structures with multiple junctions[40]. In a major advancement for the field, Rothemund introduced the concept and methodology for constructing DNA origamis by folding long, single stranded DNA molecules into arbitrary 2D shapes[41]. To make a DNA origami, a long single stranded DNA (7 kb) and over 200 short staple strands were mixed together and annealed in a single step. The staple strands hybridize to target locations on the 7 kb-long ssDNA scaffold, folding the scaffold into desired shapes of roughly 100 nm in diameter. The structures can be programmed to form different shapes (squares, disks, and stars) or to bear complex patterns on the surfaces (words and images). The smallest feature on the surface is rough 6 nm, the size of a single DNA base. This technique has been adopted by researchers to develop complex 3D structures for applications ranging from drug delivery to electronic circuit assembly[43,44]. Tikhomirov et al. reported the largest DNA origami assembly to date[45]. They used a recursive, hierarchical process to assemble a small set of unique DNA strands into a much larger

structure. Using this "fractal assembly" method, the team created micrometer-scale renderings of complex patterns such images of Mona Lisa, a rooster, and a bacterium.

DNA could also help direct the assembly of nanoparticles and form novel crystalline structures. In a remarkable paper by Rogers and Manoharan, DNA-grafted nanoparticles were first annealed to form crystal structures[46]. They controlled the strength of the colloid bonds by adding competing complementary strands and observed the crystal structure to go through phase transitions not found in atomic systems or other DNA functionalized colloids.

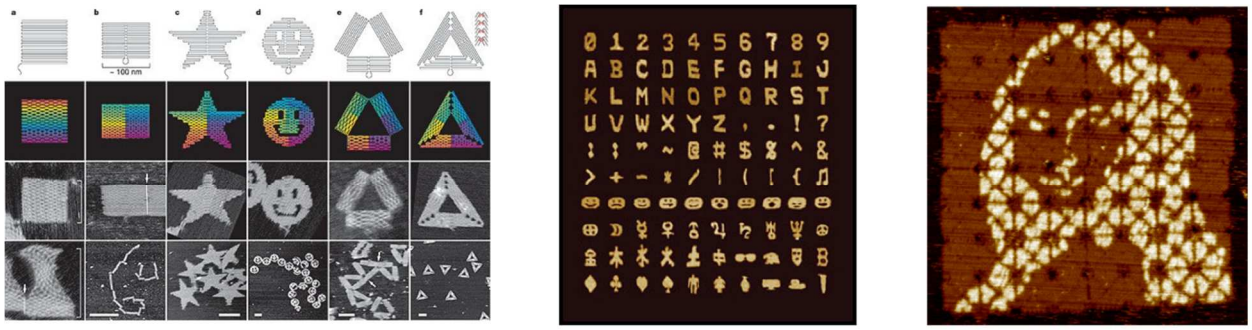

Figure 8 Programmable nanostructures made with DNA nanotechnology. Left and center: DNA origamis formed into different shapes (squares, disks, and stars) or to bear complex patterns on the surfaces (words and images). **Right:** the largest DNA origami assembly to date, created using a fractal assembly method.

3.4 DNA-based macro-structures

This section provides a short survey of macroscopic programmable structures made from DNA-based systems.

Padirac et al. reported the experimental observation of traveling waves and spirals generated by a CRN implementing the predator-prey model[47]. They constructed *de novo* an enzyme-assisted DNA circuit with tunable parameters. The velocity of the propagating wave front could be tuned by changing the network topology, reaction rate constants, and the diffusion coefficients of species. Zadorin et al. demonstrated the synthesis of a French flag pattern using a bistable network in a reaction-diffusion system[48]. Guo el al. demonstrated DNA-functionalized polyacrylamide hydrogels that exhibited pH-sensitive shape memory properties[49]. The gels were crosslinked with short DNA oligos and formed into an initial shape at a pH 5.0. When the gel was submerged in a pH 8.0 solution, it dissolved into a quasi-liquid state. However, when the hydrogel was transferred back to a pH 5.0 solution, the dissolved bonds could re-hybridize, returning the hydrogel to its original shape. Cangialosi et al. created functional hydrogels by embedding the gels with DNA strands and crosslinking the gels with photolithography[50]. They showed that the functionalized gels could undergo programmable volumetric expansion by adding complementary DNA strands to the gels, which initiated successive extensions of crosslinks. They then constructed soft machines by layering gels having different DNA sequences. When the correct complementary strands are introduced, these soft machines could be induced to display sequential shape changes.

Scalise et al. proposed a reaction-diffusion based framework for generating complex patterns by sequentially applying modular filters to an initially simple pattern, where each module would be

realized with DNA-based CRN[51]. Dalchau et al. proposed the DNA constructs for implementing chemical oscillator circuits and modeled the circuits as reaction-diffusion systems[52]. Their computer simulations show that the parameters of these circuits be tuned to exhibit Turing patterns. Chirieleison et al. implemented the first system that relied only on DNA-based reaction-diffusion to carry out macroscopic patterning[53]. They demonstrated an edge-detection system, where the DNA circuit containing photosensitive DNA strands converted UV light the outline of an input pattern.

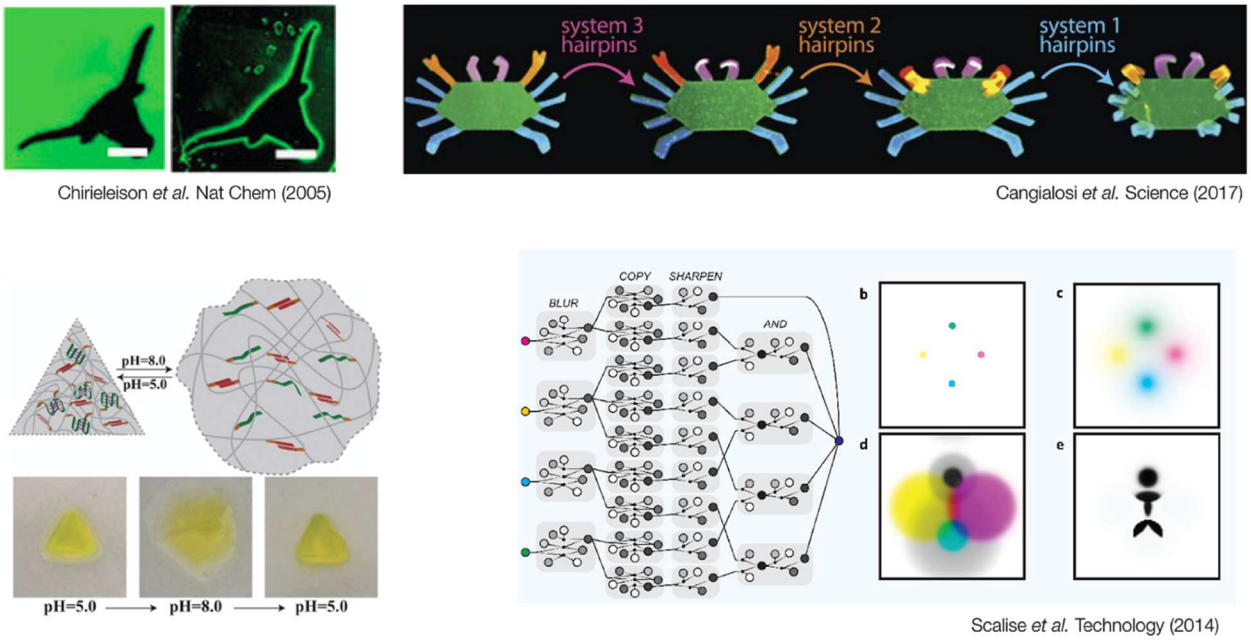

Figure 9 DNA-based macrostructures. Top left: a DNA-based, reaction-diffusion edge detection system, where photosensitive DNA strands converted UV light the outline of an input pattern. **Top right:** functional hydrogels embedded with crosslinked DNA strands that actuate via the addition of input strands. **Bottom left:** DNA-functionalized polyacrylamide hydrogels with pH-sensitive shape memory properties. **Bottom right:** a reaction-diffusion based framework for generating complex patterns by sequentially applying modular filters to an initially simple pattern

BIBLIOGRAPHY

(1) Zhang, X. A.; Yu, S.; Xu, B.; Li, M.; Peng, Z.; Wang, Y.; Deng, S.; Wu, X.; Wu, Z.; Ouyang, M.; et al. Dynamic Gating of Infrared Radiation in a Textile. *Science* **2019**, *363* (6427), 619–623. https://doi.org/10.1126/science.aau1217.

(2) Cheung, K. C.; Gershenfeld, N. Reversibly Assembled Cellular Composite Materials. *Science* **2013**, *341* (6151), 1219–1221. https://doi.org/10.1126/science.1240889.

(3) Slavkov, I.; Carrillo-Zapata, D.; Carranza, N.; Diego, X.; Jansson, F.; Kaandorp, J.; Hauert, S.; Sharpe, J. Morphogenesis in Robot Swarms. *Sci. Robot.* **2018**, *3* (25), eaau9178. https://doi.org/10.1126/scirobotics.aau9178.

(4) What's in the Bag: A Distributed Approach to 3D Shape Duplication with Modular Robots - MIT Press books https://ieeexplore-ieee-org.offcampus.lib.washington.edu/document/6578001 (accessed Jun 12, 2019).

(5) Rubenstein, M.; Payne, K.; Will, P.; Wei-Min Shen. Docking among Independent and Autonomous CONRO Self-Reconfigurable Robots. In *IEEE International Conference on Robotics and Automation, 2004. Proceedings. ICRA '04. 2004*; 2004; Vol. 3, pp 2877-2882 Vol.3. https://doi.org/10.1109/ROBOT.2004.1307497.

(6) Wei-Min Shen; Will, P. Docking in Self-Reconfigurable Robots. In *Proceedings 2001 IEEE/RSJ International Conference on Intelligent Robots and Systems. Expanding the Societal Role of Robotics in the the Next Millennium (Cat. No.01CH37180)*; 2001; Vol. 2, pp 1049–1054 vol.2. https://doi.org/10.1109/IROS.2001.976307.

(7) Sydney Gladman, A.; Matsumoto, E. A.; Nuzzo, R. G.; Mahadevan, L.; Lewis, J. A. Biomimetic 4D Printing. *Nat. Mater.* **2016**, *15* (4), 413–418. https://doi.org/10.1038/nmat4544.

(8) Ding, Z.; Yuan, C.; Peng, X.; Wang, T.; Qi, H. J.; Dunn, M. L. Direct 4D Printing via Active Composite Materials. *Sci. Adv.* **2017**, *3* (4), e1602890. https://doi.org/10.1126/sciadv.1602890.

(9) Gul, J. Z.; Sajid, M.; Rehman, M. M.; Siddiqui, G. U.; Shah, I.; Kim, K.-H.; Lee, J.-W.; Choi, K. H. 3D Printing for Soft Robotics – a Review. *Sci. Technol. Adv. Mater.* **2018**, *19* (1), 243–262. https://doi.org/10.1080/14686996.2018.1431862.

(10) Schaffner, M.; Faber, J. A.; Pianegonda, L.; Rühs, P. A.; Coulter, F.; Studart, A. R. 3D Printing of Robotic Soft Actuators with Programmable Bioinspired Architectures. *Nat. Commun.* **2018**, *9* (1), 878. https://doi.org/10.1038/s41467-018-03216-w.

(11) Zuluaga, D. C.; Menges, A. 3D Printed Hygroscopic Programmable Material Systems. *MRS Online Proc. Libr. Arch.* **2015**, *1800*. https://doi.org/10.1557/opl.2015.644.

(12) Tibbits, S. 4D Printing: Multi-Material Shape Change. *Archit. Des.* **2014**, *84* (1), 116–121. https://doi.org/10.1002/ad.1710.

(13) Direct 4D printing via active composite materials | Science Advances https://advances.sciencemag.org/content/3/4/e1602890 (accessed Jun 12, 2019).

(14) Li, W.; Matthews, C. C.; Yang, K.; Odarczenko, M. T.; White, S. R.; Sottos, N. R. Autonomous Indication of Mechanical Damage in Polymeric Coatings. *Adv. Mater.* **2016**, *28* (11), 2189–2194. https://doi.org/10.1002/adma.201505214.

(15) Jochum, F. D.; Theato, P. Temperature- and Light-Responsive Smart Polymer Materials. *Chem Soc Rev* **2013**, *42* (17), 7468–7483. https://doi.org/10.1039/C2CS35191A.

(16) Huang, W. M.; Ding, Z.; Wang, C. C.; Wei, J.; Zhao, Y.; Purnawali, H. Shape Memory Materials. *Mater. Today* **2010**, *13* (7), 54–61. https://doi.org/10.1016/S1369-7021(10)70128-0.

(17) Mao, Y.; Ding, Z.; Yuan, C.; Ai, S.; Isakov, M.; Wu, J.; Wang, T.; Dunn, M. L.; Qi, H. J. 3D Printed Reversible Shape Changing Components with Stimuli Responsive Materials. *Sci. Rep.* **2016**, *6*, 24761. https://doi.org/10.1038/srep24761.

(18) Engines of Creation - K. Eric Drexler - Google Books https://books.google.com/books?hl=en&lr=&id=BZVBDwAAQBAJ&oi=fnd&pg=PR5&dq=eric+drexler&ots=vHnnUHhkFH&sig=tPAniLbFqaJA9tfgz4NSG8iMt9Q#v=onepage&q=eric%20drexler&f=false (accessed Jun 12, 2019).

(19) Kudernac, T.; Ruangsupapichat, N.; Parschau, M.; Maciá, B.; Katsonis, N.; Harutyunyan, S. R.; Ernst, K.-H.; Feringa, B. L. Electrically Driven Directional Motion of a Four-Wheeled Molecule on a Metal Surface. *Nature* **2011**, *479* (7372), 208–211. https://doi.org/10.1038/nature10587.

(20) Palima, D.; Glückstad, J. Gearing up for Optical Microrobotics: Micromanipulation and Actuation of Synthetic Microstructures by Optical Forces. *Laser Photonics Rev.* **2013**, *7* (4), 478–494. https://doi.org/10.1002/lpor.201200030.

(21) Budrene, E. O.; Berg, H. C. Complex Patterns Formed by Motile Cells of Escherichia Coli. *Nature* **1991**, *349* (6310), 630–633. https://doi.org/10.1038/349630a0.

(22) Yamanaka, H.; Kondo, S. In Vitro Analysis Suggests That Difference in Cell Movement during Direct Interaction Can Generate Various Pigment Patterns in Vivo. *Proc. Natl. Acad. Sci.* **2014**, 201315416. https://doi.org/10.1073/pnas.1315416111.

(23) The Chemical Basis of Morphogenesis. 36.

(24) Gierer, A.; Meinhardt, H. A Theory of Biological Pattern Formation. *Kybernetik* **1972**, *12* (1), 30–39. https://doi.org/10.1007/BF00289234.

(25) Winfree, A. T. The Prehistory of the Belousov-Zhabotinsky Oscillator. *J. Chem. Educ.* **1984**, *61* (8), 661. https://doi.org/10.1021/ed061p661.

(26) Ammelt, E.; Schweng, D.; Purwins, H.-G. Spatio-Temporal Pattern Formation in a Lateral High-Frequency Glow Discharge System. *Phys. Lett. A* **1993**, *179* (4), 348–354. https://doi.org/10.1016/0375-9601(93)90690-2.

(27) Gurevich, E. L.; Zanin, A. L.; Moskalenko, A. S.; Purwins, H.-G. Concentric-Ring Patterns in a Dielectric Barrier Discharge System. *Phys. Rev. Lett.* **2003**, *91* (15), 154501. https://doi.org/10.1103/PhysRevLett.91.154501.

(28) Kogelschatz, U. Filamentary, Patterned, and Diffuse Barrier Discharges. *IEEE Trans. Plasma Sci.* **2002**, *30* (4), 1400–1408. https://doi.org/10.1109/TPS.2002.804201.

(29) Wolpert, L. Positional Information and the Spatial Pattern of Cellular Differentiation. *J. Theor. Biol.* **1969**, *25* (1), 1–47. https://doi.org/10.1016/S0022-5193(69)80016-0.

(30) Basu, S.; Gerchman, Y.; Collins, C. H.; Arnold, F. H.; Weiss, R. A Synthetic Multicellular System for Programmed Pattern Formation. *Nature* **2005**, *434* (7037), 1130. https://doi.org/10.1038/nature03461.

(31) Liu, C.; Fu, X.; Liu, L.; Ren, X.; Chau, C. K. L.; Li, S.; Xiang, L.; Zeng, H.; Chen, G.; Tang, L.-H.; et al. Sequential Establishment of Stripe Patterns in an Expanding Cell Population. *Science* **2011**, *334* (6053), 238–241. https://doi.org/10.1126/science.1209042.

(32) Dupin, A.; Simmel, F. C. Signalling and Differentiation in Emulsion-Based Multi-Compartmentalized in Vitro Gene Circuits. *Nat. Chem.* **2019**, *11* (1), 32. https://doi.org/10.1038/s41557-018-0174-9.

(33) Gines, G.; Zadorin, A. S.; Galas, J.-C.; Fujii, T.; Estevez-Torres, A.; Rondelez, Y. Microscopic Agents Programmed by DNA Circuits. *Nat. Nanotechnol.* **2017**, *12* (4), 351–359. https://doi.org/10.1038/nnano.2016.299.

(34) Zhang, D. Y.; Winfree, E. Control of DNA Strand Displacement Kinetics Using Toehold Exchange. *J. Am. Chem. Soc.* **2009**, *131* (47), 17303–17314. https://doi.org/10.1021/ja906987s.

(35) Seelig, G.; Soloveichik, D.; Zhang, D. Y.; Winfree, E. Enzyme-Free Nucleic Acid Logic Circuits. *Science* **2006**, *314* (5805), 1585–1588. https://doi.org/10.1126/science.1132493.

(36) Zhang, D. Y.; Turberfield, A. J.; Yurke, B.; Winfree, E. Engineering Entropy-Driven Reactions and Networks Catalyzed by DNA. *Science* **2007**, *318* (5853), 1121–1125. https://doi.org/10.1126/science.1148532.

(37) Soloveichik, D.; Seelig, G.; Winfree, E. DNA as a Universal Substrate for Chemical Kinetics. *Proc. Natl. Acad. Sci.* **2010**, *107* (12), 5393–5398. https://doi.org/10.1073/pnas.0909380107.

(38) Qian, L.; Winfree, E.; Bruck, J. Neural Network Computation with DNA Strand Displacement Cascades. *Nature* **2011**, *475* (7356), 368–372. https://doi.org/10.1038/nature10262.

(39) Chen, Y.-J.; Dalchau, N.; Srinivas, N.; Phillips, A.; Cardelli, L.; Soloveichik, D.; Seelig, G. Programmable Chemical Controllers Made from DNA. *Nat. Nanotechnol.* **2013**, *8* (10), 755–762. https://doi.org/10.1038/nnano.2013.189.

(40) Seeman, N. C. DNA in a Material World. *Nature* **2003**, *421* (6921), 427. https://doi.org/10.1038/nature01406.

(41) Rothemund, P. W. K. Folding DNA to Create Nanoscale Shapes and Patterns. *Nature* **2006**, *440* (7082), 297–302. https://doi.org/10.1038/nature04586.

(42) Zhang, Q.; Jiang, Q.; Li, N.; Dai, L.; Liu, Q.; Song, L.; Wang, J.; Li, Y.; Tian, J.; Ding, B.; et al. DNA Origami as an *In Vivo* Drug Delivery Vehicle for Cancer Therapy. *ACS Nano* **2014**, *8* (7), 6633–6643. https://doi.org/10.1021/nn502058j.

(43) Maune, H. T.; Han, S.; Barish, R. D.; Bockrath, M.; Iii, W. A. G.; Rothemund, P. W. K.; Winfree, E. Self-Assembly of Carbon Nanotubes into Two-Dimensional Geometries Using DNA Origami Templates. *Nat. Nanotechnol.* **2010**, *5* (1), 61–66. https://doi.org/10.1038/nnano.2009.311.

(44) Liu, J.; Geng, Y.; Pound, E.; Gyawali, S.; Ashton, J. R.; Hickey, J.; Woolley, A. T.; Harb, J. N. Metallization of Branched DNA Origami for Nanoelectronic Circuit Fabrication. *ACS Nano* **2011**, *5* (3), 2240–2247. https://doi.org/10.1021/nn1035075.

(45) Tikhomirov, G.; Petersen, P.; Qian, L. Fractal Assembly of Micrometre-Scale DNA Origami Arrays with Arbitrary Patterns. *Nature* **2017**, *552* (7683), 67–71. https://doi.org/10.1038/nature24655.

(46) Rogers, W. B.; Manoharan, V. N. Programming Colloidal Phase Transitions with DNA Strand Displacement. *Science* **2015**, *347* (6222), 639–642. https://doi.org/10.1126/science.1259762.

(47) Padirac, A.; Fujii, T.; Estévez-Torres, A.; Rondelez, Y. Spatial Waves in Synthetic Biochemical Networks. *J. Am. Chem. Soc.* **2013**, *135* (39), 14586–14592. https://doi.org/10.1021/ja403584p.

(48) Zadorin, A. S.; Rondelez, Y.; Gines, G.; Dilhas, V.; Urtel, G.; Zambrano, A.; Galas, J.-C.; Estevez-Torres, A. Synthesis and Materialization of a Reaction–Diffusion French Flag Pattern. *Nat. Chem.* **2017**, *9* (10), 990–996. https://doi.org/10.1038/nchem.2770.

(49) Guo, W.; Lu, C.-H.; Orbach, R.; Wang, F.; Qi, X.-J.; Cecconello, A.; Seliktar, D.; Willner, I. PH-Stimulated DNA Hydrogels Exhibiting Shape-Memory Properties. *Adv. Mater.* **2015**, *27* (1), 73–78. https://doi.org/10.1002/adma.201403702.

(50) Cangialosi, A.; Yoon, C.; Liu, J.; Huang, Q.; Guo, J.; Nguyen, T. D.; Gracias, D. H.; Schulman, R. DNA Sequence–Directed Shape Change of Photopatterned Hydrogels via High-Degree Swelling. *Science* **2017**, *357* (6356), 1126–1130. https://doi.org/10.1126/science.aan3925.

(51) Scalise, D.; Schulman, R. Designing Modular Reaction-Diffusion Programs for Complex Pattern Formation. *TECHNOLOGY* **2014**, *02* (01), 55–66. https://doi.org/10.1142/S2339547814500071.

(52) Dalchau, N.; Seelig, G.; Phillips, A. Computational Design of Reaction-Diffusion Patterns Using DNA-Based Chemical Reaction Networks. In *DNA Computing and Molecular Programming*; Murata, S., Kobayashi, S., Eds.; Lecture Notes in Computer Science; Springer International Publishing, 2014; pp 84–99.

(53) Chirieleison, S. M.; Allen, P. B.; Simpson, Z. B.; Ellington, A. D.; Chen, X. Pattern Transformation with DNA Circuits. *Nat. Chem.* **2013**, *5* (12), 1000–1005. https://doi.org/10.1038/nchem.1764.

Chapter 4 DNA-based IFFL modules for periodic stripe pattern formation

Abstract

Artificial systems with the capacity for spatial self-organization and metamorphosis would be immensely useful as they could alter their form or composition based on perceived environmental cues. Biological organisms achieve spatial self-organization through vast and complex networks of chemical reactions that regulate cell processes and control the flow of matter and information at the molecular level. Similarly, it is possible that artificial systems could use synthetic chemical reactions to generate controlled pattern formation. Specifically, each layer of our circuit can be broken down into an IFFL (incoherent feedforward loop) module, an amplifier module, and a threshold module. Different combinations of modules can manifest in a variety of spatial-temporal behaviors such as single pulse, dual pulses, or oscillations. Under this design architecture, a pattern of concentric rings could conceivably be made by cascading together multiple IFFLs, which are known pulse-generators. Neighboring IFFLs are connected by amplifier modules, which help prevent signal damping over time. We exploit this modularity to individually tune, test, and characterize circuits and the corresponding dynamics. We show the design and experimental implementation of a DNA-based circuit with emergent ringed pattern formation in agarose gel media, demonstrate control over the appearance of rings by adjusting the concentrations of embedded circuit components, and report our results on the observations of dual-pulse dynamics produced by a cascaded-IFFL circuit and the potential observation of damped oscillations.

4.1 Introduction

Dynamic pattern formation is ubiquitous in nature. We see it in animals that use camouflage to avoid detection by predators, and in plants whose growth follows geometries optimal for photosynthesis. Such capacity for spatial metamorphosis is also desirable in artificial systems designed to autonomously alter their form or composition based on perceived environmental cues. Biological organisms regulate cell processes by controlling the flow of matter and information at the molecular level, through vast and complex networks of chemical reactions. Similarly, artificial systems could use synthetic chemical reactions to manipulate matter at the nanometer and micrometer scales to produce controlled pattern formation.

Advances in atomic and molecular self-assembly enable humans to exert extremely fine-tuned control over the spatial arrangements of matter at incredibly short length scales[1,2]. However, nano self-assembly relies on local interactions and does not exhibit large scale pattern emergence, which results from coordinated behaviors between interacting molecules. In order to engineer dynamic self-organizing systems, we need to look beyond localized molecule-to-molecule recognition, to how chemical reactions happening at the nanoscale give rise to emergent pattern formation at the macroscale. Reaction-diffusion has been proposed as a potential mechanism underlying morphogenesis and pattern formation in biological organisms[3,4]. Macroscopic pattern emergence and spatial oscillations have also been observed in several synthetic RD systems, including Turing patterns in far-from-equilibrium chemical reactors[5], and stripe formations and traveling waves in systems involving gene networks and enzymatic reactions[6-8]. However, capacities for control over the resulting spatial patterns in these systems are often limited.

DNA is inherently programmable and ideal for nanoscale information processing. Chemical computers constructed out of DNA have shown sophisticated problem solving capabilities[10,11], and DNA strand displacement can in theory be used to implement arbitrarily complex chemical reaction networks (CRNs)[12,13]. Aside from its computational prowess, DNA is also a material of choice for molecular construction. At the nanoscale, DNA has been used to create programmable, dynamic 3D nanostructures[14], and DNA origami can potentially facilitate the self-assembly of any pre-programmed shape[2].

The programmability of DNA is also beginning to be exploited to create reaction diffusion patterns with macroscale dimensions. For example, enzyme-assisted DNA reactions were shown to develop dynamic nonlinear behaviors such as traveling waves[15], and an enzyme-free DNA circuit was shown to perform complex spatial computation like edge detection[16]. Further, in silico work suggests the possibility of DNA implemented CRNs for self-organization of complex patterns[17]. Most importantly, DNA reactions are much more deterministic than any other types of molecular interactions due to the precision of Waston-Crick base-pairing. Thus, in contrast to synthetic chemical reactors, a system designed to harness the programmability of DNA for pattern formation would have unparalleled degree of control over a great variety of patterns[18]. However, to date, we have yet to see the experimental realization of a DNA-based system capable of autonomously generating tunable, macroscopic spatial patterns. In this paper, we report our work on the construction of a self-contained, DNA based reaction-diffusion system capable of sustaining tunable spatial oscillations in a 2D gel reactor. To achieve this, we follow a modular design process that translates abstract spatial pattern to DNA strand displacement reactions. Specifically, we show the design and experimental implementation of a DNA-based circuit with emergent ringed pattern

formation in an agarose gel media and demonstrate control over the appearance of rings by adjusting the concentrations of embedded circuit components.

4.2 Modular design approach for translating pattern into DNA circuit

Here, we will develop a systematic approach to engineer patterns of concentric rings using DNA strand displacement. A multi-ring pattern can be broken down into smaller features, i.e. a series of individual rings, which makes it ideal as a toy model for testing a modular design approach. At the reaction network level, we will realize each ring as an incoherent feed-forward loop and then demonstrate that multiple such motifs can be connected in series. Previous work on pattern formation using engineered gene circuits in colonies of bacteria6 suggests that such a strategy can result in robust ring formation in synthetic cellular systems, but so far, this approach has not been realized to create macroscale patterns in non-living molecular systems. To prevent signal damping over time, we place a linear amplifier between a pair of neighboring IFFLs, such that the amount of trigger available to each IFFL remains similar throughout. We take advantage of modularity to individually tune, tested, and characterized circuits and their corresponding spatial manifestations. Network description of a IFFL is shown in Fig 2a). Reporter signal (S1) is both directly activated and indirectly inhibited by the trigger (I1). We design DNA circuit such that each reaction pathway in the network is represented by a strand displacement reaction. Here we make the distinction between different types of circuit components to help organize our circuit. Messenger strands (MS) are single stranded oligonucleotides that help propagate information and connects otherwise orthogonal reactions to each other. Messenger gates (MG) are duplexes that serve as vessels for inactive messenger strands, which are activated when the gates interact with the appropriate free-floating messenger strands. Functional strands (FS) are single stranded oligos functionalized with

molecules (such as fluorophores) to perform an observable function (e.g. fluoresce). Functional gates (FG) are duplexes that affect the observable effects of function strands by either producing or interacting with (e.g. quenching) the strands. For clarity, only single strands are represented in the schematics, as only they are capable of inducing reactions. In the IFFL, MS1 (I1) triggers the release of both signal strand FS1 (S1) and MS2. MS2 activates FG1, which subsequently quenches the now free floating FS1. Since it only takes one reaction for signal activation, but two reactions for signal inhibition, the time difference between the two pathways results in the signal being re-quenched only after it has already reached high fluorescence levels.

Like in other pattern forming synthetic systems5-7,20, we use the concentrations of circuit components as a tunable knob for changing the appearance, such as thickness and intensity, of rings (Fig 2). A narrower, less intense pulse can result from either a low concentration of activator (MS1) or a high concentration of inhibitor (MG2). Further, the choice of component to tune also affect the profile of the resulting pulse. Tuning the activator results in a pulse where the activation and inhibition of signal are proportionally tuned at similar rates (Fig2) since changing the activator concentration directly affects the signal gate and messenger gate MG2 (Fig 2b). Tuning the inhibitor results in a pulse where the inhibition is much more affected than the activation (Fig2) since the activation pathway is not directly affected by changes in MG2 concentrations (Fig 2b). Spatially, these differences would manifest as a ring with smooth edges for i. and with a sharp inner edge for ii. (Fig 2c).

Spatial experiments are carried out in an agarose gel media (Fig 3). All components except MS1 were first mixed together in a low density (0.25%) agarose gel solution at 40oC to minimize

denaturing of duplexes. A low-density gel was chosen to best approximate free solution. The gel solution is placed in a 2 cm x 2 cm x 0.4 cm (width x height x depth) reactor chamber to solidify. A small cavity is punched into the center of the solidified gel for insertion of MS1, which initiates the reactions cascades as it diffuses into the gel. Finally, the gel reactor is covered to prevent evaporation and imaged at set time intervals.

Three sets of experiments were conducted in gels embedded with signal gate only (Fig 4a), signal and inhibitor gates (Fig 4b), and signal and excess inhibitor gates (Fig 4c). We observe that the width and intensity of rings decrease when the concentration of inhibitors in the reactors is higher, similar to how pulses grew narrower in the in-solution experiments.

4.3 Cascading multiple DNA modules

Next, we expand the circuit to generate multiple rings. An obvious way to achieve this is to sequentially connect multiple orthogonal IFFLs. However, as reactions take place, the number of messenger strands at any step will be smaller than that of the previous step, because the reactions used to create the IFFL are non-catalytic and a fraction of the input is consumed. Without signal restoration, the signal is thus damped over time. To counter this, place an amplifier between sequential IFFLs such that for each round of reaction, only the trigger messenger strand gets amplified. The the overall circuit design is kept minimal by adding only one extra amplifier per IFFL and the modularity of the circuit remains intact as each IFFL would be kinetically identical.

We chose to use linear fixed-gain, rather than catalytic, amplifiers to minimize leak, simplify circuit design and reduce reaction time. Effectively, the amplifier takes one messenger

strand (MS2) from the first IFFL as an input and outputs multiple messenger strands (MS4) for triggering of the next IFFL (Fig 4a). Specifically, we enable 3X amplification by building each amplifier gate to carry three identical trigger strands. Amplification takes place through a two-step reaction. First, the short MS2 strand is translated into the much longer strand, MS3 (Fig 4b). Then MS3 reacts with the amplifier gate to release three trigger strands (Fig 4c). Further, we intentionally build a delay into the system by designing MS2 to react much more slowly with MG3 than it does with FG to slow down the triggering of the second IFFL and improve the resolution between neighboring rings.

Next, we tested the amplifier module by connecting it to an IFFL at one end and a signal gate at the other. A working amplifier should trigger the succeeding signal to a similar level as the preceding signal. The same FAM fluorophore was used for both signal strands, so the spectrometry measurements show a sum of two signals. In-solution experiments show the amplifier working as expected, indicated by the signal being restored to 1X fluorescence level after an initial drop (Fig 4d). Further, we demonstrate modularity of the system by showing that when components in the first ring are tuned, as when we vary the concentration of inhibitor in the first module alone, its corresponding signal experiences a significant drop in fluorescence, while the second signal is much less affected (Fig 4d lines 1 vs 2, and 3 vs 4). Similarly, when we vary concentration of signal gates in module 2, signal of module 1 is affected to a much lesser degree in comparison (Fig 4d lines 1 vs 3, and 2 vs 4).

4.4 Discussion

In this paper, we constructed and characterized a de novo DNA-based system for emergent pattern formation of two-dimensional ring structures. Specifically, we used the concentration of circuit components as tuning knobs for programming the thickness, intensity and edge sharpness of rings. Our system is different from other stripe-forming reactors in that our modular design architecture enables compartmentalized programming of features by tuning components within modules, providing a much greater degree of control over pattern geometries. We believe that a model-guided approach is needed to fully realize the potential of our system. Toward this end, we need to establish the quantitative relationships necessary for modeling by analyzing reaction kinetics and diffusion coefficients in our current experimental results.

As patterns become more complicated, it is desirable to optimize the circuit for size and simplicity. Since many different circuit designs could conceivably lead to similar patterns, even for simple patterns like those explored in this work, our circuit design is likely not optimal. DNA circuit design remains an art that relies on a combination of experience, ingenuity and trial and error. However, the design space of more complex patterns can quickly become unwieldy for explorations by hand. We plan on building an automated workflow that will translate a pattern, with specified intensity and geometry, into suitable DNA strand displacement circuits. This could potentially enable exploration of design spaces beyond simple patterns like rings, waves and spots, to include a greater variety of shapes. The information gleaned from here will help us explore self-organization in biological systems. We can easily substitute fluorophores with other functional molecules to perform a variety of operations. Can develop dynamic patterns that change upon the introduction of a new reactant or exposure to new stimuli.

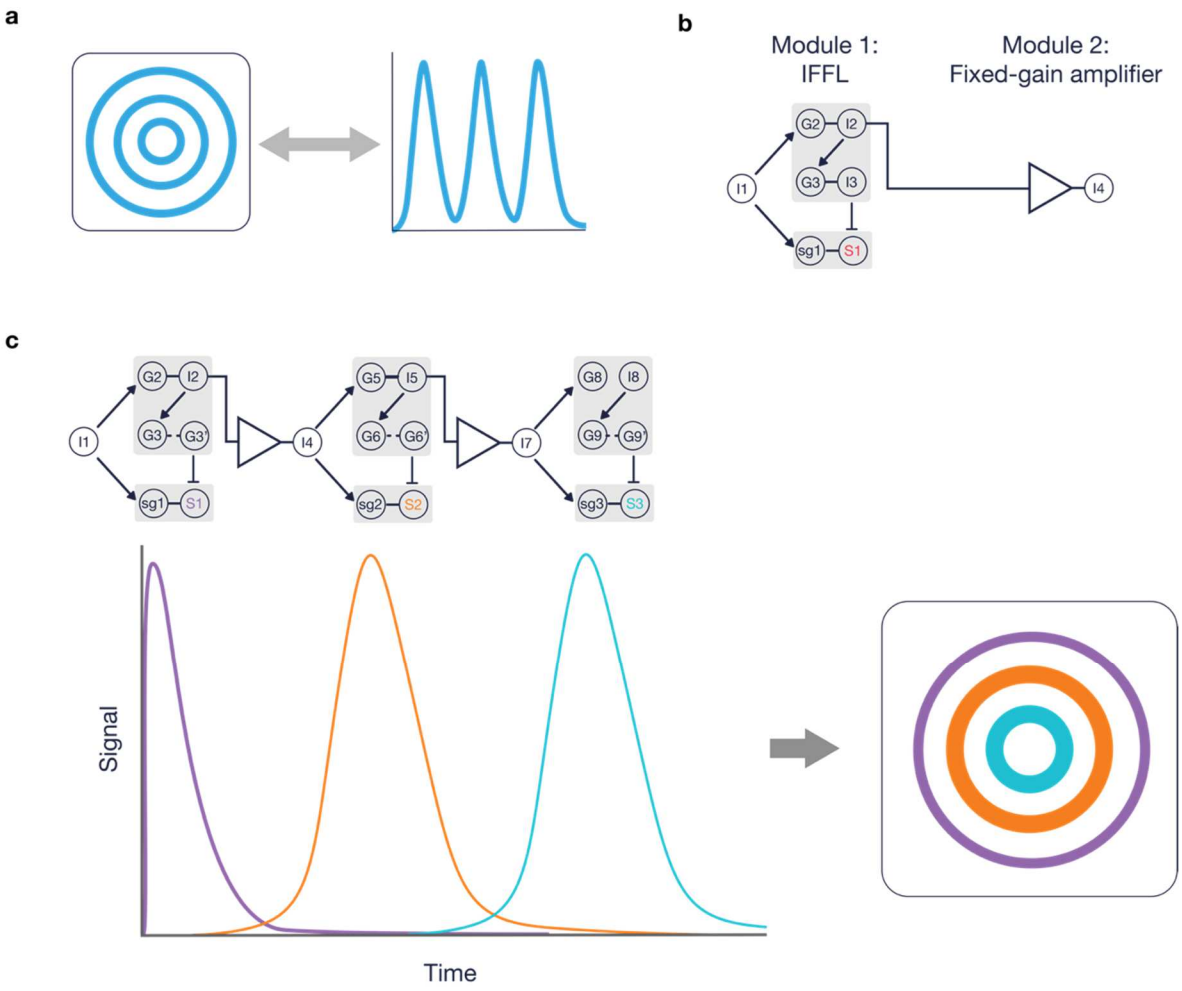

Figure 1: **Modular design process for translating spatial pattern to chemical reaction network representation. a,** a spatial pattern is transformed into corresponding temporal profile to elucidate design choices. For example, oscillatory signal can be broken down into individual pulses. **b,** we design two modules to construct a single layer ring circuit. The first module is, an incoherent feedforward loop (IFFL), is responsible for pulse-generation. The amplifier module connects IFFLs together and prevents damping over time through signal restoration. **c,** multiple pulses and rings can be generated by connected identically designed modules in series.

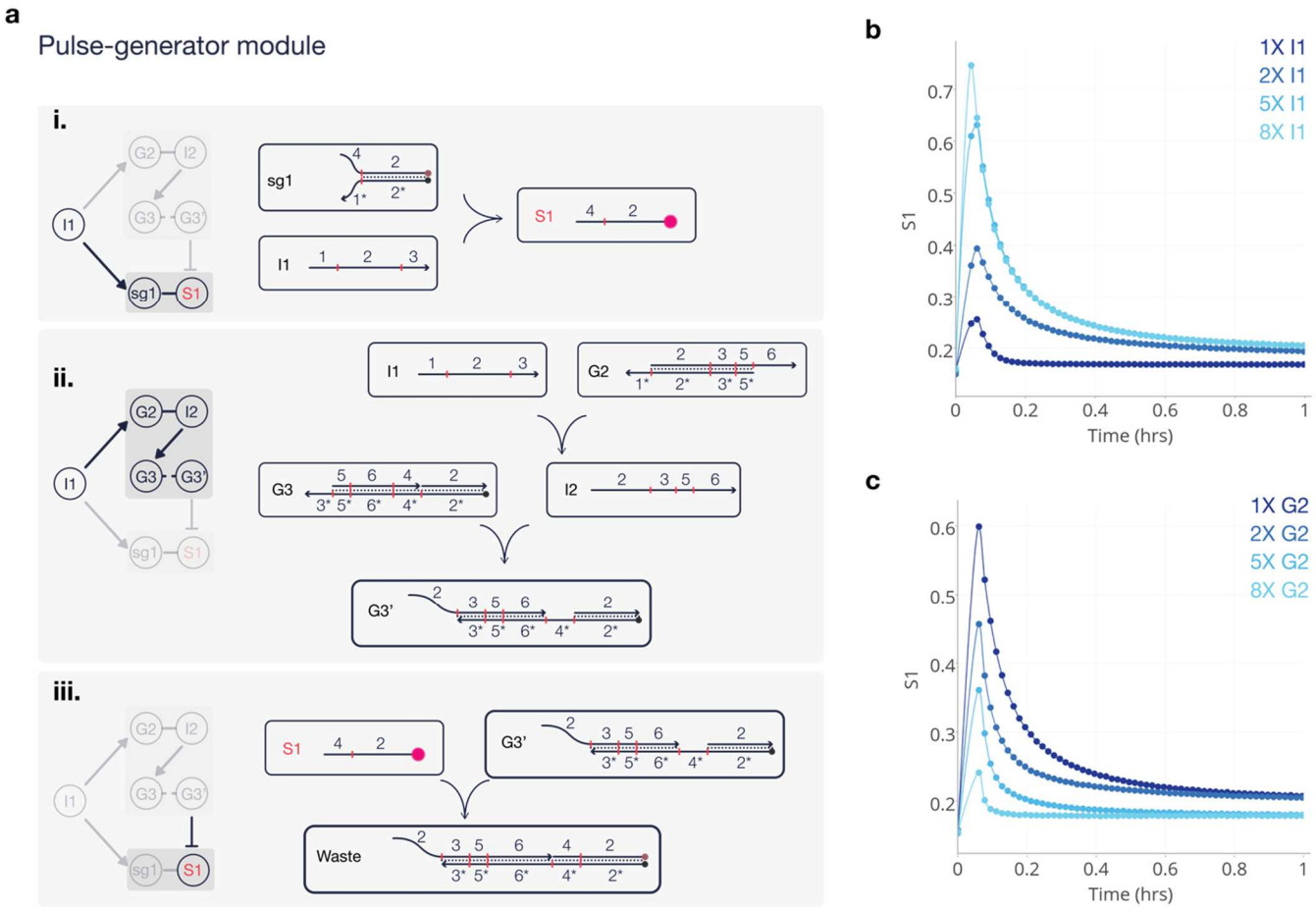

Figure 2: **Design and implementation of a single pulse generating circuit. a,** the IFFL is broken down into individual reaction pathways and their corresponding strand displacement implementations. b and c, in-solution experiments of single pulse circuit showing that tuning different circuit components leads to programmable responses of the resulting pulse.

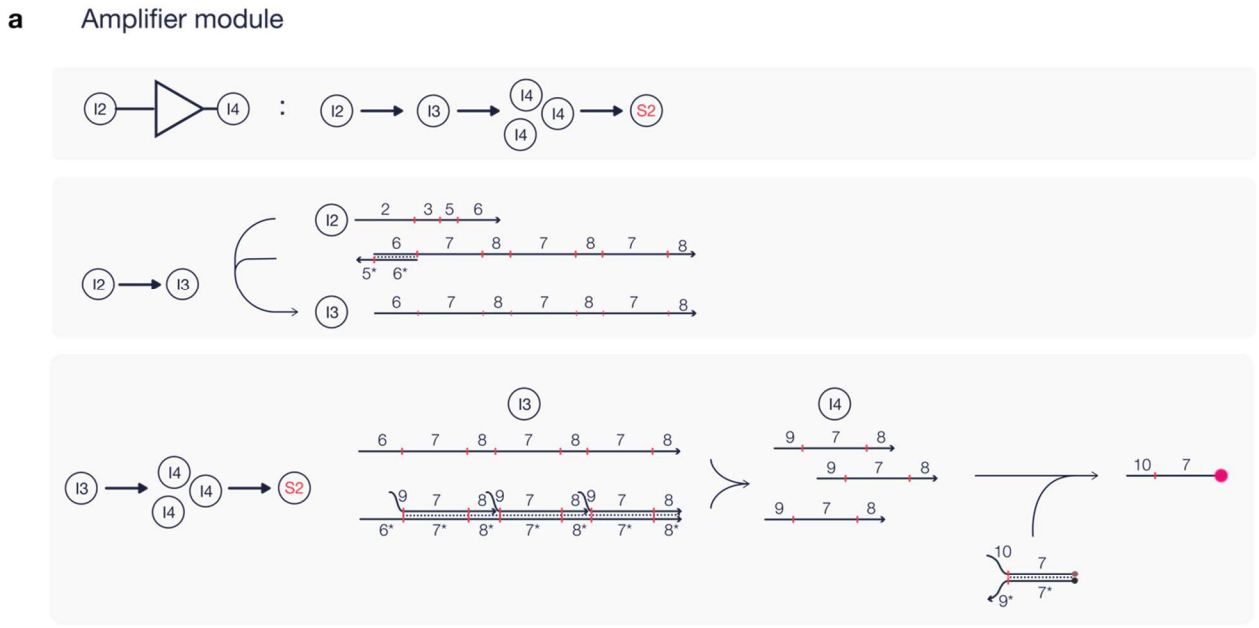
a
Amplifier module
I2
I4
I3
S2
2 3 5 6
6 7 8 7 8 7 8
5* 6*
9 7 8
10 7
9* 7*

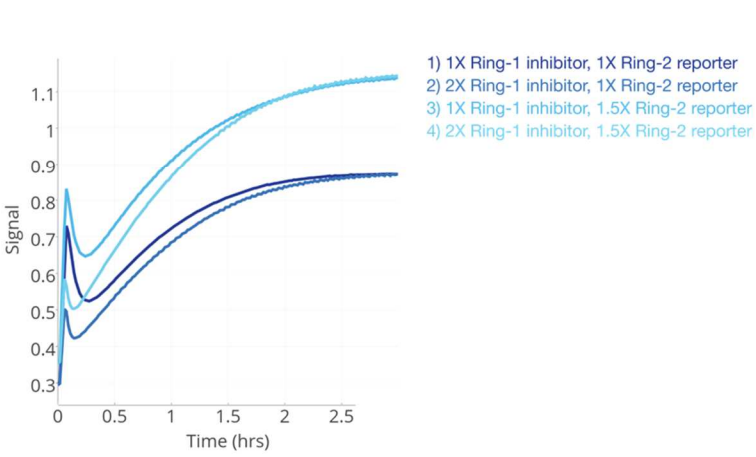
b
1) 1X Ring-1 inhibitor, 1X Ring-2 reporter
2) 2X Ring-1 inhibitor, 1X Ring-2 reporter
3) 1X Ring-1 inhibitor, 1.5X Ring-2 reporter
4) 2X Ring-1 inhibitor, 1.5X Ring-2 reporter
Signal
Time (hrs)

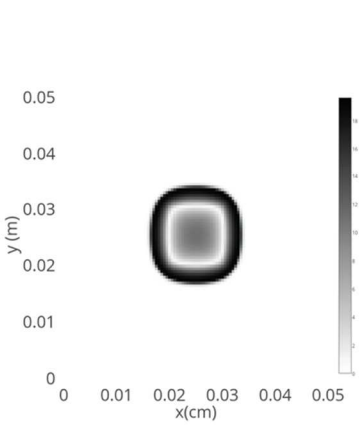
c
y (m)
x(cm)

BIBLIOGRAPHY

1. Eigler, D. M. & Schweizer, E. K. Positioning single atoms with a scanning tunnelling microscope. Nature **344,** 524–526 (1990).
2. Rothemund, P. W. K. Folding DNA to create nanoscale shapes and patterns. Nature **440,** 297–302 (2006).
3. Turing, A. M. The Chemical Basis of Morphogenesis. Philos. Trans. R. Soc. B Biol. Sci. **237,** 37–72 (1952).
4. Gierer, A. & Meinhardt, H. A theory of biological pattern formation. Kybernetik **12,** 30–39 (1972).
5. De Kepper, P., Castets, V., Dulos, E. & Boissonade, J. Turing-type chemical patterns in the chlorite-iodide-malonic acid reaction. Phys. D Nonlinear Phenom. **49,** 161–169 (1991).
6. Basu, S., Gerchman, Y., Collins, C. H., Arnold, F. H. & Weiss, R. A synthetic multicellular system for programmed pattern formation. Nature **434,** 1130–1134 (2005).
7. Liu, C. et al. Sequential Establishment of Stripe Patterns in an Expanding Cell Population. Science (80-.). **334,** (2011).
8. Padirac, A., Fujii, T., Estévez-Torres, A. & Rondelez, Y. Spatial Waves in Synthetic Biochemical Networks. J. Am. Chem. Soc. **135,** 14586–14592 (2013).
9. Nicolis, Gregoire, and Ilya Prigogine. Self-organization in nonequilibrium systems. Vol. 191977. Wiley, New York, 1977.
10. Adleman, L. Molecular computation of solutions to combinatorial problems. Science (80-.). **266,** (1994).
11. Qian, L., Winfree, E. & Bruck, J. Neural network computation with DNA strand displacement cascades. Nature **475,** 368–372 (2011).
12. Soloveichik, D., Seelig, G. & Winfree, E. DNA as a universal substrate for chemical kinetics. Proc. Natl. Acad. Sci. U. S. A. **107,** 5393–8 (2010).
13. Chen, Y.-J. et al. Programmable chemical controllers made from DNA. Nat. Nanotechnol. **8,** 755–762 (2013).
14. Rogers, W. B. & Manoharan, V. N. Programming colloidal phase transitions with DNA strand displacement. Science (80-.). **347,** (2015).
15. Zadorin, A. S., Rondelez, Y., Galas, J.-C. & Estevez-Torres, A. Synthesis of Programmable Reaction-Diffusion Fronts Using DNA Catalyzers. Phys. Rev. Lett. **114,** 68301 (2015).

16. Chirieleison, S. M., Allen, P. B., Simpson, Z. B., Ellington, A. D. & Chen, X. Pattern transformation with DNA circuits. Nat Chem **5,** 1000–1005 (2013).
17. Dalchau, N., Seelig, G. & Phillips, A. in 84–99 (Springer, Cham, 2014).
18. Scalise, D. & Schulman, R. Designing modular reaction-diffusion programs for complex pattern formation. TECHNOLOGY **2,** 55–66 (2014).
19. Mangan, S. & Alon, U. Structure and function of the feed-forward loop network motif. Proc. Natl. Acad. Sci. U. S. A. **100,** 11980–5 (2003).
20. Basu, S., Mehreja, R., Thiberge, S., Chen, M.-T. & Weiss, R. Spatiotemporal control of gene expression with pulse-generating networks. Proc. Natl. Acad. Sci. U. S. A. **101,** 6355–60 (2004).

Chapter 5 Programmable patterns in a DNA-based reaction-diffusion system

Abstract

Biology offers compelling proof that macroscopic "living materials" can emerge from reactions between diffusing biomolecules. Here, we show that molecular self-organization could be a similarly powerful approach for engineering functional synthetic materials. We introduce a programmable DNA-hydrogel that produces tunable patterns at the centimeter length scale. We generate these patterns by implementing chemical reaction networks through synthetic DNA complexes, embedding the complexes in hydrogel, and triggering with locally applied input DNA strands. We first demonstrate ring pattern formation around a circular input cavity and show that the ring width and intensity can be predictably tuned. Then, we create patterns of increasing complexity, including concentric rings and non-isotropic patterns. Finally, we show "destructive" and "constructive" interference patterns, by combining several ring-forming modules in the gel and triggering them from multiple sources. We further show that computer simulations based on the reaction-diffusion model can predict and inform the programming of target patterns.

5.1 Introduction

Programmable matter research aims to engineer functional materials that can autonomously transform their appearances or physical properties in response to environmental stimuli and user-defined inputs. Top down methods like 3D-printing have enabled the development of shapeshifting biomimetic constructs that are sensitive to heat, light, or water[3,10]. Advances in micro-robotics have led to modular robotic swarms that can self-organize into two- and three-dimensional

structures[5,11]. But we are still far from creating true programmable matter. Currently, synthetic materials and systems either rely on components too large to be integrated into material fabrics, as with modular robot systems, or have limited functions, as with 3D printed materials.

Chemical computing offers a tantalizing alternative. Biological patterning processes like camouflaging and morphogenesis suggest that complex and environmentally responsive systems could arise from the self-organization of information-bearing agents like molecules or cells[12,13]. Engineering molecular systems to predictably form complex patterns like those seen in biology would clearly have significant implications for programmable materials research.

The mathematical model of reaction-diffusion provides a framework for designing and engineering programmable structures through chemical computing[13–15]. In this model, spatial patterns can emerge from local interactions between diffusing agents[16]. Simulations developed within this framework have successfully replicated complex biological patterns[17,18], suggesting a path toward model-guided engineering of autonomous self-organizing systems. However, experimental *de novo* realizations of pattern formation have been sparse.

Early examples of synthetic pattern formation include the Belousov-Zhabotinsky (BZ) chemical oscillator[19,20], which generates macroscopic spatiotemporal patterns via a series of redox reactions. While the mechanics of BZ reactions are well understood, we cannot control reaction kinetics or program the resulting patterns to display target behaviors. Synthetic biologists have genetically engineered quorum-sensing bacteria to create stripes and traveling waves[21–23]. Such results showcase the potential of a biochemical approach to programming self-organized pattern

formation, but the precision of patterning is still limited because the engineered reaction networks operate in a background of evolved and not fully understood cellular machinery. Cell-free biochemical reaction networks are another promising alternative but systems engineered to date, although capable of generating a wide range of patterns in aqueous reactors[24–27], still largely rely on catalysis of evolved enzymes and have limited programmability.

DNA is unique, even among biopolymers, in that interactions are quantitatively predictable and follow the rules of Watson-Crick base pairing[28,29]. DNA origami and related self-assembly technologies take advantage of this predictability for the construction of 2- and 3-dimensional objects of varying sizes and complexity[30,31]. This work has culminated in macroscopic materials with nanometer-scale addressability. But these periodic crystals[32] or random gels[33,34] lack non-trivial long-range order and are expensive because DNA acts as the primary structural component. Thus, to recapitulate the diversity and scale of biological patterns and materials with DNA alone we still need to develop approaches that extend to the centimeter scale and beyond.

To address this need, recent work has begun to explore the feasibility of DNA-only reaction-diffusion patterns[35]. Toehold-mediated DNA strand displacement has proved to be a convenient framework for implementing complex reaction sequences using synthetic DNA in well-mixed test tubes[36,37]. Using the principles of strand displacement, researchers have created sophisticated reaction networks that perform computation like neural networks[38,39], diagnostic classifiers[40], dynamic 3D nanostructures[41,42] and even approximate the dynamics of formal, mathematically specified chemical reaction networks (CRNs)[43–46]. Building on these results, theoretical work has argued that a wide range of patterns is achievable if DNA-based CRNs are embedded in a spatial

reactor[47,48]. Chirieleison *et al.* took an important step toward experimentally demonstrating pattern formation with DNA strand displacement-based CRNs and engineered an edge detection system[49]. However, despite the advances made in these projects, the state of art for programming macroscopic features still lags that of their microscopic counterparts.

Here, we report the design and synthesis of a novel DNA-hydrogel hybrid material for programmable spatial patterning at the centimeter length scale. Patterns are generated via the reaction-diffusion of DNA complexes separately embedded in porous hydrogel and predefined cavities in the gel. Using this system, patterns of varying geometries can be generated and quantitatively tuned by controlling the reaction rates of species. To further demonstrate programmability, we show that the dynamic behavior of these spatial patterns can be predicted by computer simulations.

5.2 Constructing a pulse-generator

Figure 1 shows the workflow of our DNA-based programmable patterning system. A simple ring-forming module forms the basic building block for all other patterns realized in this work (**Figure 1A**). Rings are an archetype for studying synthetic pattern formation[21,23] and, as we will show, form an ideal starting point for generating more complex patterns. To implement this module, we begin by formulating a pulse-generating CRN (**Fig. 1B**). We then realize this CRN using DNA strand displacement-based complexes (**Fig. 1C**). Next, we synthesize the DNA-hydrogel by suspending these DNA complexes in an agarose solution and molding the mixture into thin sheets. Finally, we load initiator strands into cavities in the DNA-hydrogel to trigger programmed pattern formation (**Fig. 1D**). A predictive spatial model built in Visual DSD informs the concentrations of

initiator strands required for generating target patterns. Input parameters for the model include reaction constants and diffusion coefficients inferred from spectrometry and gel experiments (**Fig. 1D**). Depending on the initial conditions (concentrations of initiating strands) and boundary conditions (shape and placement of cavities), gels embedded with identical DNA gates can be programmed to display a variety of spatial dynamics (**Fig. 1E**).

The core CRN for pulse formation consists of three reactants: activator, reporter, and inhibitor (**Fig. 2A**). An activator is a single-stranded DNA molecule used to initiate a reaction cascade. A reporter is a partially double-stranded DNA complex with a fluorophore-labeled signal (top) strand and a quencher-labeled bottom strand that is fully complementary to the activator. An inhibitor is a partially double-stranded DNA complex with an unmodified protector strand and a longer quencher strand that is fully complementary to the signal strand (**Fig. 2B**). We entered the desired domain structures into NUPACK Design to generate compatible sequences for building the pulse module (**Supplementary Section 1**). These sequences are listed in **Supplementary Table 1**. In a well-mixed setting, this three-component reaction module produces a single pulse via a two-step reaction (**Fig. 2B**): first, activators trigger fluorescence by releasing signal strands from reporters through toehold-meditated strand displacement; then, the signal is absorbed and repressed by the inhibitor.

To test the pulse module, we added reporter and inhibitor to a solution, triggered the reaction by adding the activator, and measured fluorescence changes using a spectrofluorometer. As designed, we can program the pulse shape by changing reactant concentrations. Specifically, pulse amplitude and duration depend on the rates of signal activation and inhibition: when we lowered the activator-

to-inhibitor ratio in the solution, we observed a corresponding decrease in pulse amplitude and duration (**Fig. 2C**).

We developed a computational model in Visual DSD to simulate the pulse module (**Supplementary Sections 2 and 3**). The model consists of two reversible bimolecular reactions: signal activation (activator and reporter react to produce signal) and signal inhibition (signal is absorbed by inhibitor). Model parameters include reaction rate constants of signal activation and inhibition, as measured from separate spectrometry experiments (**Supplementary Figs. 1-4**). Our simulation confirms the module as a pulse generator (**Fig. 2C**) and further refines the rate constants to improve prediction accuracy (**Supplementary Section 3, Supplementary Table 2**).

5.3 Programming single-ring patterns

Next, we set out to test spatial pattern formation. We synthesized DNA-hydrogel sheets by suspending reporters in 0.7% agarose solution. We used low melting point agarose and added reporter gates at room temperature to minimize denaturing. We cast the gels into thin sheets by pouring the mixed solutions into acrylic reactors. **Supplementary Figs. 5 and 6** illustrate this process in detail.

To initiate pattern formation, we loaded activators and inhibitors into a circular cavity at the center of the DNA-hydrogel sheet (**Fig. 2D**). As the diffusion fronts of activators and inhibitors advance, they react with the embedded reporters to trigger an outwardly propagating pulse, leading to the formation of a ring pattern. Thus, the ring pattern is a direct result of the interplay between diffusion and reaction. **Fig. 2E** shows the formation of a ring pattern over the course of 6 hours.

Additionally, radially averaged intensity profiles provide quantitative information about pattern geometry not readily discernable from gel images alone. We found that the width and peak intensity of the ring grow over time as reporters are being triggered (**Fig. 2F**).

Like the amplitude and duration of a signal pulse measured in a well-mixed solution, the intensity and width of a ring also depend on the initial conditions of the DNA-hydrogel sheet. Reducing the initial concentration of activators resulted in rings with decreased widths and peak intensities (**Fig. 2G**). Radially averaged intensity profiles show that the inhibitor concentration controls the position of the trailing edge (**Fig. 2H**), while the activator concentration controls the position of the leading edge (**Fig. 2I**). To make meaningful comparisons, we established standard curves to convert fluorescence values to concentration units for spectrometry and gel image data (**Supplementary Figs. 7 and 8**).

Using Visual DSD, we built a predictive reaction-diffusion model to simulate pattern formation (**Supplementary Section 4**). The model uses rate constants inferred from spectrometry data (**Supplementary Table 2**) and assumes a common diffusion coefficient for all DNA complexes in our gel matrix (derivation of the diffusion coefficient is described in detail in **Supplementary Section 2** and **Supplementary Fig. 9**). The simulation results are displayed alongside corresponding gel images and show good quantitative agreement with the experimentally observed patterns (**Fig. 2G**).

5.4 Building tunable concentric rings

Next, we asked whether we could control the radius of the ring pattern by adding a threshold component to our core CRN. The threshold is a single-stranded DNA that is fully complementary to the activator (**Fig. 3A**). Because hybridization between the activator and the threshold is faster than the reaction between the activator and the reporter, the threshold effectively acts as a sink to the activator.

To study the effect of threshold in a spatial setting, we embedded threshold along with reporters in the hydrogel (**Fig. 3B**). Activators diffusing into the gel are annihilated upon encountering the threshold. Thus, signal activation only occurs once a region has been depleted of unreacted threshold. We prepared gels embedded with different threshold concentrations (**Fig. 3C, Supplementary Fig. 10**). We found that for gels triggered with identical activator and inhibitor concentrations, higher threshold concentrations reduced the radius proportionally; for gels embedded with a nonzero amount of threshold, decreasing the activator concentration also reduced ring radius, but less effectively than increasing the threshold **(Fig. 3D**). Here, we define the radius as the distance between the position of peak intensity and the center of the gel, as measured from radially averaged intensity profiles (**Supplementary Fig. 10**). We updated our predictive computational model to include the threshold, using empirically derived rate constants and diffusion coefficient (**Supplementary Fig. 11**). Comparisons between the radially averaged intensity profiles of gel images and spatial simulations show that the simulation performs well for predicting ring patterns under different initial conditions (**Supplementary Fig. 12**).

Leveraging our ability to program the ring radius, we proceeded to build programmable patterns of two concentric rings. We designed a second ring-forming module with the same components as the first module but orthogonal sequences (**Supplement Section 1, Supplementary Table 1**). Next, we combined the reporters for these two modules, labeled M1 and M2, in the same hydrogel and added threshold for M2 only (**Fig. 3E**). We prepared twelve DNA-hydrogels, corresponding to four M2 threshold and three M2 activator concentration levels (**Fig. 3F**), while maintaining the same concentrations of M1 components across all twelve gels. To trigger pattern formation, we loaded both M1 and M2 activators and inhibitors in the cavity. The outer ring's radius remained largely unchanged across experiments. Meanwhile, the inner ring's radius was proportional to the levels of activator and threshold, with high activator and low threshold values corresponding to larger radii (**Fig. 3G**). For gels without the threshold, we found that changing M2 activator concentrations alone had no effect on the radius of the inner ring (**Fig. 3G**), further validating the essential role of threshold for changing ring radius.

To better visualize the two-ring patterns, we replaced the FAM fluorophore in M2 with Cy5, such that M1 and M2 signals have distinct colors. We used this improved visualization to show that it is possible to program the order in which the rings appear. Using the same setup as the previous experiment, we prepared two gels containing either M1 threshold (**Fig. 3I**) or M2 threshold (**Fig. 3I**), but not both. The gels were subjected to identical conditions otherwise. In Gel I, M1 signal activation lags M2 signal activation, resulting in an orange ring (FAM, M1) encircled by a blue ring (Cy5, M2). In Gel II, the order of the rings is reversed. Alternatively, we embedded two gels with both M1 and M2 threshold and triggered them with either higher M1 activator (**Fig. 3I**) or

higher M2 activator (**Fig. 3II**). This experiment shows that we can program the order of rings by either varying the concentration of initiator strands or the composition of the DNA hydrogel.

5.5 Beyond isotropic patterns

So far, we have only considered programmable pattern formation with isotropic boundary conditions. Next, we went beyond this simple geometry and generated anisotropic patterns by changing the shapes and placements of cavities. First, we loaded activators into an "X" shaped cavity in a gel embedded with only reporters (**Fig. 4A**). Because reaction rates are proportional to the concentration of reactants, this gel configuration resulted in high signal at the center and low signal at the tips (**Fig. 4A**). We then amplified the asymmetry by embedding threshold in the hydrogels and, separately, by changing the angles between the legs of the X-shaped cavity. Adding threshold amplifies the time difference between signal activation at the tips and at the center, while decreasing the angle increases activator concentration in the interior of the angle, which leads to faster signal activation.

We prepared nine DNA-hydrogels divided into three groups based on their embedded threshold concentrations. Each group was further divided into three gels based on the angles in the "X" cavity on the gel (**Fig. 4B**). We measured the distance from the vertex to the center of the gel for different time points, cavity angles, and threshold concentrations (**Fig. 4C**). We also plotted the vertex distances for different time points and fitted the data to Fick's equation to find the "effective diffusion coefficient", a reaction-diffusion dependent parameter we use to quantify the speed of signal propagation (**Supplementary Fig. 15**). For the same angle, both vertex distance (at the last

time point) and the effective diffusion coefficient show an approximately linear dependence in threshold concentration (**Fig. 4D**).

Finally, we generated ring interference patterns by placing cavities at multiple locations in the gel. **Supplementary Table 3** lists the setup of each experiment in detail. Gels I-IV in **Fig. 4D** were synthesized from the same DNA-hydrogel solution containing M1 and M2 reporters. We applied different initial and boundary conditions to each gel to generate distinct patterns. For gel I, we loaded M1 activators and inhibitors in both cavities. We found that signals interfered destructively in regions where the rings intersected. This happens because the areas enclosed by the rings are devoid of reporters but are replete with inhibitors. Hence, as the two rings emanating from different cavities collide, their signal strands get consumed by the inhibitors from the opposite cavity. In contrast, when we loaded one of the cavities with M2 activators and inhibitors, we observed constructive interference of signals because the two diffusion fronts carry orthogonal reactants. Gel III was configured to display a combination of constructive and destructive signal interference. We created 3 cavities for gel IV. The center cavity was loaded with circuit 1 activators and inhibitors; the two peripheral cavities were loaded with circuit 1 inhibitors only. Since the signal and inhibitor diffusion fronts will annihilate each other wherever they collide, the resulting pattern is an incomplete ring with openings facing the directions of the peripheral cavities. **Supplementary Fig. 15** shows gels V and VI, where we used color coding and thresholding to induce two orthogonal rings of different radii that intersect.

5.6 Discussion

We demonstrated a new approach to engineering programmable materials at the macroscale, using the reaction and diffusion of synthetic DNA strands to achieve quantitative and modular control over spatial patterns in hydrogels. To show proof of concept, we focused on a relatively simple pattern generated by non-catalytic CRNs. Incorporating more complex reaction networks, such as introducing feedback and cascading mechanisms, would produce more varied patterns[47]. We could also control diffusion by embedding appropriate complementary strands in the hydrogel to selectively slow down the diffusion of target DNA complexes, a possibility that has been explored in previous work[50]. Similar mechanisms could be used to convert transient patterns into permanent patterns by immobilizing signal strands with complementary capture sequences. Our system still relies on external spatial input and is therefore not fully autonomous and self-organizing. However, it is conceivable that a similar approach could be used to realize Turing patterns by combining nonlinear dynamics with control over diffusion rates.

Scalise *et al.* proposed making complex DNA-based programmable patterns by sequentially applying modular filters to an initially simple input pattern[48]. Our work has taken steps toward experimentally realizing such systems by predictably transforming simple input patterns into more complex output patterns. Thus, the workflow presented here can serve as an experimental basis for future projects exploring more complicated patterning systems.

In the longer term, we foresee applications where integrating chemical computing with additive manufacturing could expand the functionalities of existing 3D printed biomimetic materials. One could also imagine substituting fluorophores with other functional molecules, such as

nanoparticles[51] and quantum dots[52], to synthesize novel materials with useful properties. Our work expands on previous research efforts in synthetic chemistry, synthetic biology, and DNA nanotechnology. Yet, we have only scratched the surface of the great array of programmable, macroscopic patterns and structures achievable by a synthetic DNA-based reaction-diffusion system. We believe this research presents a convincing case for using chemical computing in developing programmable matter.

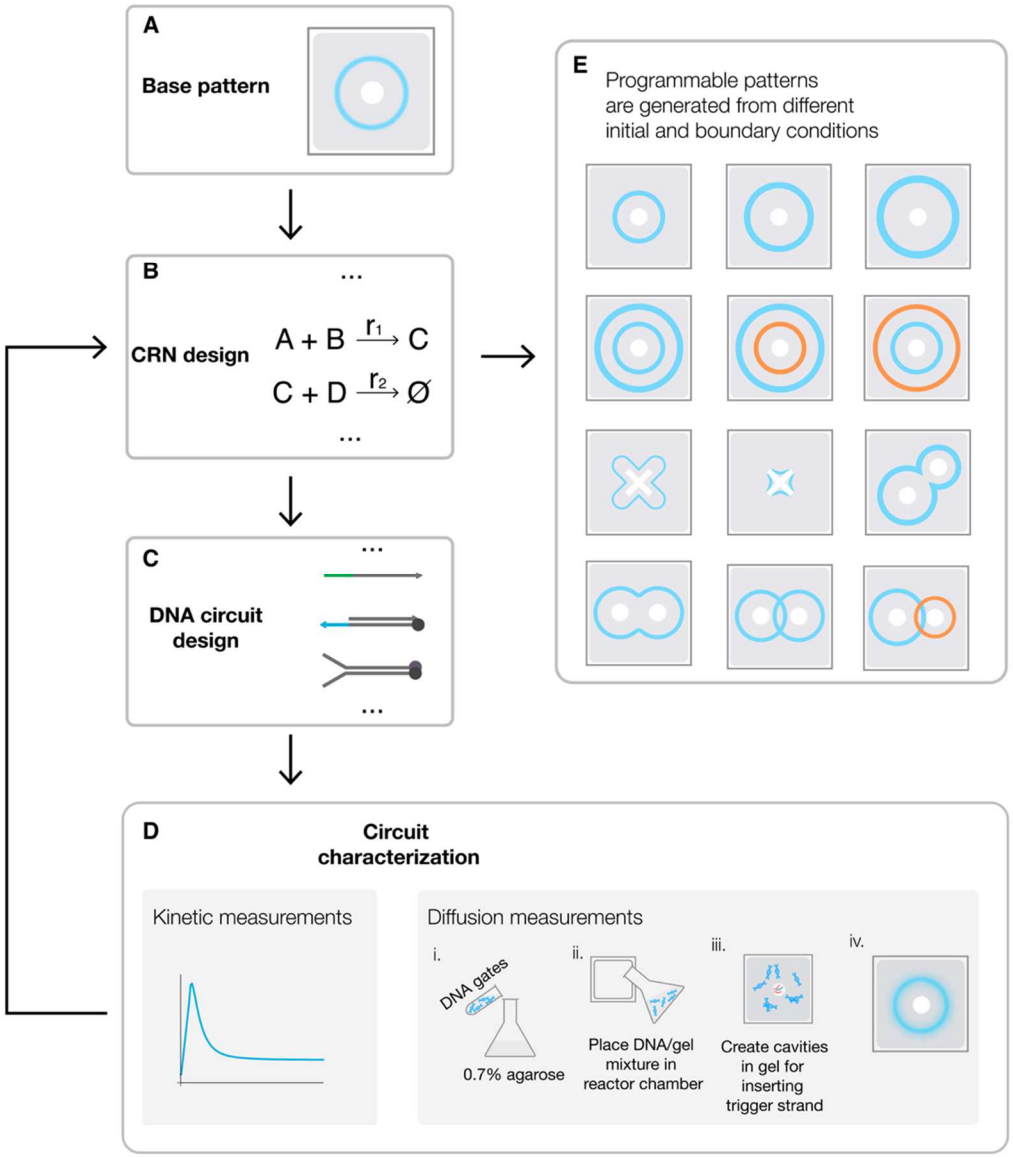

Figure 1. Overview of the workflow for DNA-based programmable patterning. A. We use a ring as the test case and basic building block for pattern formation. **B.** We designed a CRN to implement this basic pattern. **C.** The CRN is compiled into molecules that realize the desired reaction. **D.** We performed experiments both in solution and in gel. Spectrometry experiments were used to measure parameters such as reaction constants and diffusion coefficients. These parameters were then entered as input to computer simulations for predicting the spatial dynamics of the system. The model also helps us to determine the initial conditions required for generating ringed patterns with target geometries. Gel measurements were conducted by suspending DNA gates in a hydrogel solution and molding the mixture into thin sheets in a cast. To trigger programmed pattern formation, we loaded initiator strands into cavities in the DNA-hydrogel. Depending on the initial (concentrations of initiator strands) and boundary (shape and placement of cavities) conditions, gels embedded with identical DNA gates can be programmed to display different spatial dynamics. **E**. More complex patterns can be constructed by combining multiple ring-forming systems. The reaction diffusion model makes it possible to quantitatively simulate pattern formation before experimental implementation.

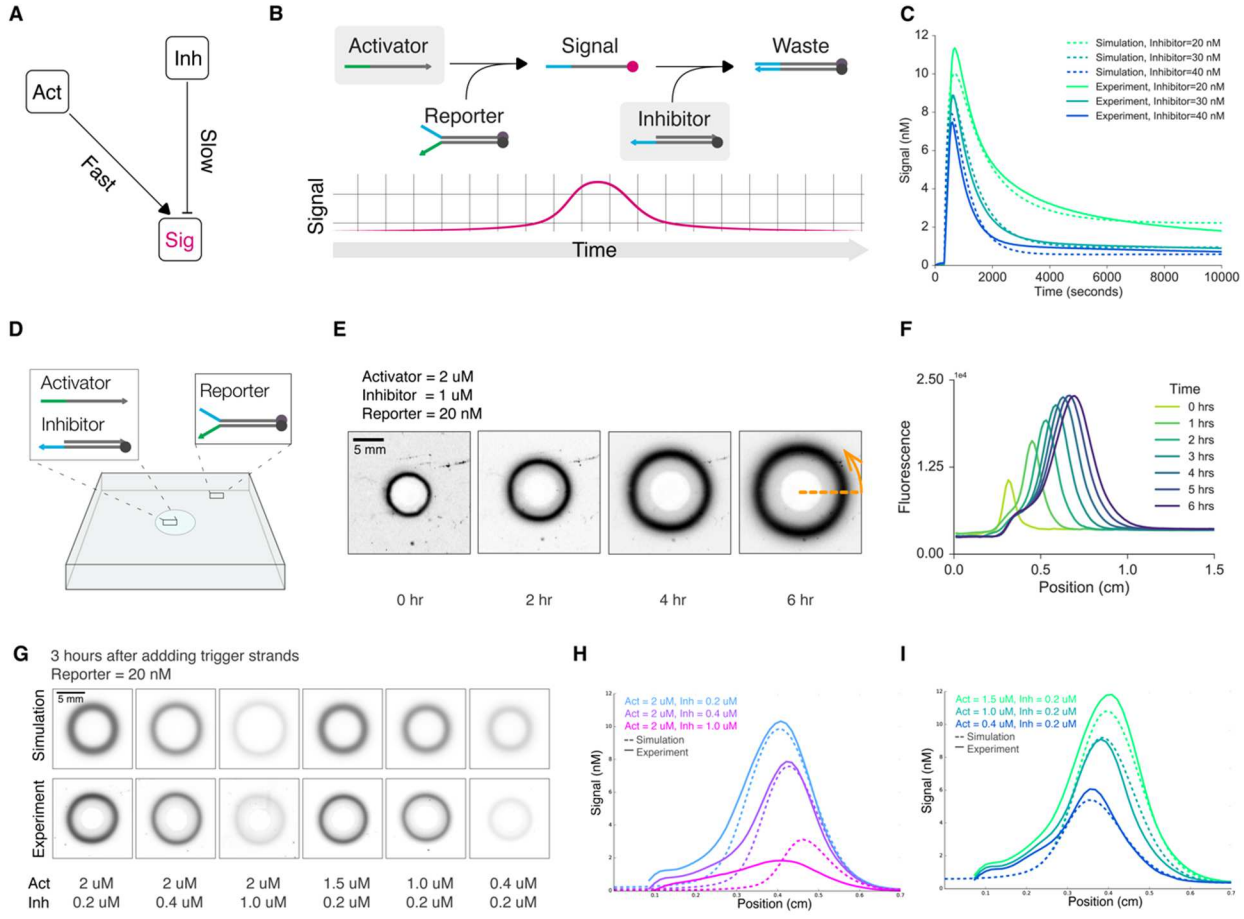

Figure 2 Single-ring pattern formation in a DNA-hydrogel. **A.** CRN for a pulse generator. Here, activators trigger the release of signals, while inhibitors repress signals. We designed the CRN such that signal activation always precedes signal inhibition. **B.** DNA strand displacement implementation of the CRN. Activators react with reporters to release signal strands. Fluorophores on the signal strands become unquenched as they disengage from reporter complexes. Free floating signal strands can be absorbed by inhibitors, which suppress signals by quenching fluorophores. Because signal activation and inhibition occur sequentially, the observed fluorescent signal forms a pulse in time. **C.** Fluorospectrometry measurement of the DNA module (activator = 100 nM, reporter = 20 nM). Solid and dashed lines indicate experimental and fitted data, respectively. The duration and amplitude of the pulse can be tuned by varying the ratio of activators to inhibitors in the system. **D.** Configuration of the hydrogel experiment. A mixture of hydrogel and reporters was molded into a square sheet. A small circular cavity was made in the center of the sheet, where we loaded activators and inhibitors. **E.** Gel images showing a circular stripe pattern developing over the course of 6 hours. **F.** Intensity profiles of the same gel experiment. The intensity profiles were obtained by taking the radially averaged intensity of gels at different time points. **G.** Varying the geometries of the single-ring pattern by changing the activator-to-inhibitor ratio. Top row: simulation results. Bottom row: gel experiment results. **H.** Varying inhibitor concentration while keeping activator concentration constant. **I.** Varying activator concentration while keeping inhibitor concentration constant.

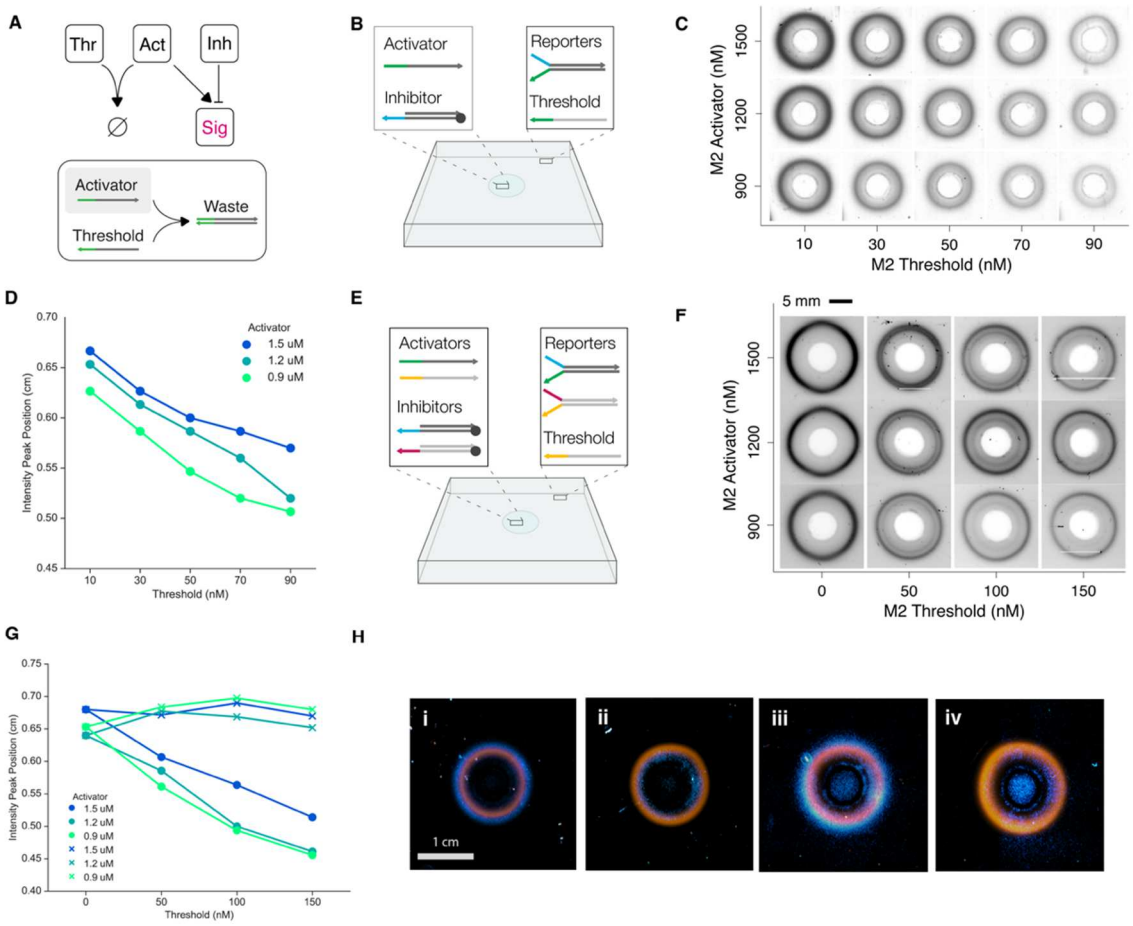

Figure 3 Tunable two-ring pattern formation. A. Schematics showing the pulse generating CRN and the corresponding DNA circuit modified to include a thresholding mechanism. Threshold strands act as sinks for activators to slow down the release of signals. **B.** Gel experiment setup for single-ring pattern with threshold. The hydrogel sheet is embedded with reporters and threshold. Activators and inhibitors are added to the circular cavity in the center of the sheet. **C.** Images showing gels embedded with five threshold concentrations at three activator concentrations. Inhibitor concentrations were set at 200 nM for every gel. Images were taken 3 hours after triggering. **D.** Intensity peak positions of threshold gel experiments. Increasing threshold concentration decreases ring radius. Changing the activator concentration has a visible, but much smaller effect on the radius. **E.** Gel experiment setup for concentric ring patterns. Each hydrogel is embedded with reporters from two orthogonal modules and threshold from only one module. To trigger the gel, we loaded the cavity with activators and inhibitors from both circuits. **F.** Images of concentric ring patterns in gels with two orthogonal modules. Each gel was synthesized according to the setup in **E**. We varied the threshold and activator concentrations for module M2 (reporter = 20 nM, inhibitor = 200 nM), while keeping concentrations for module M1 unchanged across gels (reporter = 20 nM, inhibitor = 200 nM, activator = 1200 nM). **G.** Intensity peak positions of concentric ring experiments. Peak positions for rings generated by module M1 (shown in "x" markers) remain stable across experiments, while peak positions for rings generated by module M2 (shown in circles) decrease linearly with increasing threshold. **H.** Programming the size and color of concentric ring patterns. We modified M2 such that its reporters are functionalized with Cy5 (in cyan) to differentiate it from M1 (FAM, in orange). We could selectively program the radius of a ring in a concentric ring pattern by controlling the concentration of threshold (gels 1 and 2). Changing the activator concentration has a similar, but smaller, effect, so long as the gels contain non-zero concentrations of threshold (gels 3 and 4).

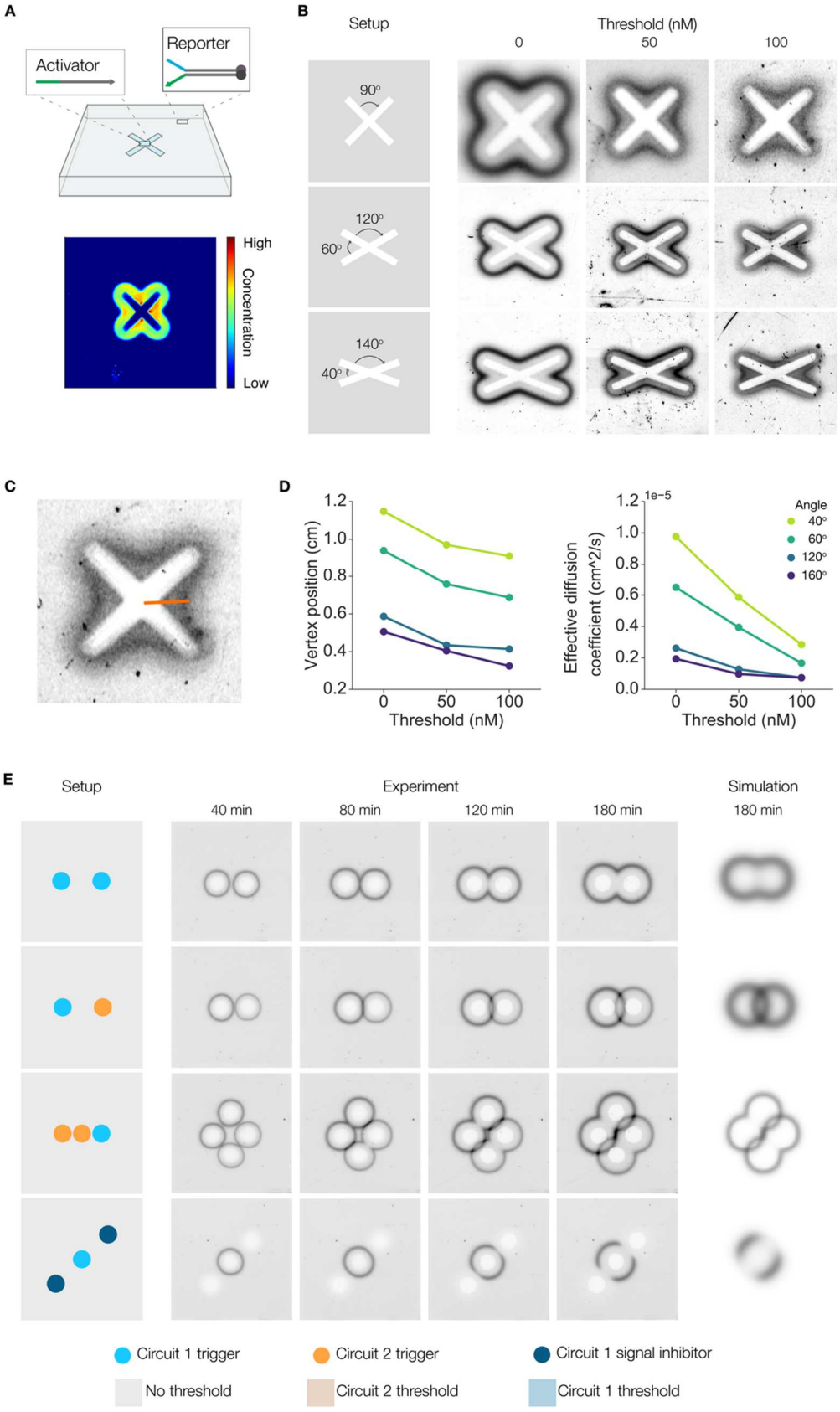
A
Activator
Reporter
High
Concentration
Low
B
Setup
Threshold (nM)
0
50
100
90°
120°
60°
140°
40°
C
D
Vertex position (cm)
Threshold (nM)
Effective diffusion coefficient (cm^2/s)
1e−5
Angle
40°
60°
120°
160°
E
Setup
Experiment
Simulation
40 min
80 min
120 min
180 min
180 min
Circuit 1 trigger
Circuit 2 trigger
Circuit 1 signal inhibitor
No threshold
Circuit 2 threshold
Circuit 1 threshold

Figure 4 Programmed patterning from variations in boundary conditions. A. Asymmetrical cavities lead to non-isotropic concentration gradient in areas immediately surrounding the cavities. Points of greater curvature see higher concentrations of initiator strands. When activators were pipetted into an X-shaped cavity punctured on a gel containing only reporter gates (top), the resulting gel image (bottom) shows higher signal activation near the center than at the tips. **B.** The degree of asymmetry can be tuned by changing the level of threshold or the angle of curvature at the center. Higher threshold concentration results in a larger lag between signal activation times at the center than at the tips. Smaller angles of curvature lead to higher concentrations of initiator strands in the interior of the angle, which results in faster signal activation. **C.** We use the distance between the vertex and center of the gel as a proxy for how fast signal gets activated for each of the conditions tested. **D.** The diffusion coefficients were derived from measuring the distance between a signal vertex and the center at different time points (left). The dependence of the effective diffusion coefficients on threshold levels and angles of curvature is shown in the right plot. **E**. Patterns can also be programmed via the content and placement of cavities. We can induce conditional interference between signal fronts by changing the types and concentrations of initiator strands in the cavities. Gels I-IV were cast from the same DNA-hydrogel mixture yet evolved distinct patterns because they had different initial and boundary conditions. The DNA complexes loaded into each cavity are color coded and shown at the bottom of the figure.

BIBLIOGRAPHY

1. Raviv, D. *et al.* Active printed materials for complex self-evolving deformations. *Sci. Rep.* (2014).
2. Sydney Gladman, A., Matsumoto, E. A., Nuzzo, R. G., Mahadevan, L. & Lewis, J. A. Biomimetic 4D printing. *Nat. Mater.* **15,** 413–418 (2016).
3. Yim, M. *et al.* Modular self-reconfigurable robot systems [Grand challenges of robotics]. *IEEE Robot. Autom. Mag.* (2007).
4. Rubenstein, M., Cornejo, A. & Nagpal, R. Programmable self-assembly in a thousand-robot swarm. *Science* (2014).
5. Hanlon, R. Cephalopod dynamic camouflage. *Current Biology* (2007).
6. Koch, A. J. & Meinhardt, H. Biological pattern formation: From basic mechanisms to complex structures. *Rev. Mod. Phys.* (1994).
7. Turing, A. M. The Chemical Basis of Morphogenesis. *Philos. Trans. R. Soc. B Biol. Sci.* **237,** 37–72 (1952).
8. Kondo, S. & Miura, T. Reaction-diffusion model as a framework for understanding biological pattern formation. *Science* (2010).
9. Gierer, A. & Meinhardt, H. A theory of biological pattern formation. *Kybernetik* (1972).
10. Pearson, J. E. Complex patterns in a simple system. *Science* (1993).
11. Yang, L. & Epstein, I. R. Oscillatory Turing Patterns in Reaction-Diffusion Systems with Two Coupled Layers. *Phys. Rev. Lett.* (2003).
12. Zaikin, A. N. & Zhabotinsky, A. M. Concentration wave propagation in two-dimensional liquid-phase self-oscillating system. *Nature* (1970).
13. Yashin, V. V. & Balazs, A. C. Pattern formation and shape changes in self-oscillating polymer gels. *Science* (2006).
14. Basu, S., Gerchman, Y., Collins, C. H., Arnold, F. H. & Weiss, R. A synthetic multicellular system for programmed pattern formation. *Nature* **434,** 1130–1134 (2005).
15. Tabor, J. J. *et al.* A Synthetic Genetic Edge Detection Program. *Cell* (2009).
16. Liu, C. *et al.* Sequential Establishment of Stripe Patterns in an Expanding Cell Population. *Science* **334,** (2011).
17. Padirac, A., Fujii, T., Estévez-Torres, A. & Rondelez, Y. Spatial waves in synthetic

biochemical networks. *J. Am. Chem. Soc.* (2013).

18. Zadorin, A. S. *et al.* Synthesis and materialization of a reaction-diffusion French flag pattern. *Nat. Chem.* (2017).
19. Gines, G. *et al.* Microscopic agents programmed by DNA circuits. *Nat. Nanotechnol.* **12,** 351–359 (2017).
20. Dupin, A. & Simmel, F. C. Signalling and differentiation in emulsion-based multi-compartmentalized in vitro gene circuits. *Nat. Chem.* **11,** 32–39 (2019).
21. Bloomfield, V. A., Crothers & D. M., Tinoco, I. J. *Nucleic Acids: Structures, Properties, and Functions*. (University Science Books, 2000).
22. SantaLucia, J. & Hicks, D. The Thermodynamics of DNA Structural Motifs. *Annu. Rev. Biophys. Biomol. Struct.* (2004).
23. Rothemund, P. W. K. Folding DNA to create nanoscale shapes and patterns. *Nature* **440,** 297–302 (2006).
24. Seeman, N. C. Nanomaterials Based on DNA. *Annu. Rev. Biochem.* (2010).
25. Zheng, J. *et al.* From molecular to macroscopic via the rational design of a self-assembled 3D DNA crystal. *Nature* (2009).
26. Um, S. H. *et al.* Enzyme-catalysed assembly of DNA hydrogel. *Nat. Mater.* (2006).
27. Lee, J. B. *et al.* Multifunctional nanoarchitectures from DNA-based ABC monomers. *Nat. Nanotechnol.* (2009).
28. Simmel, F. C. & Schulman, R. Self-organizing materials built with DNA. *MRS Bull.* **42,** 913–919 (2017).
29. Zhang, D. Y. & Winfree, E. Control of DNA strand displacement kinetics using toehold exchange. *J. Am. Chem. Soc.* (2009).
30. Zhang, D. Y. & Seelig, G. Dynamic DNA nanotechnology using strand-displacement reactions. *Nat. Chem.* (2011).
31. Qian, L., Winfree, E. & Bruck, J. Neural network computation with DNA strand displacement cascades. *Nature* (2011).
32. Cherry, K. M. & Qian, L. Scaling up molecular pattern recognition with DNA-based winner-take-all neural networks. *Nature* (2018).
33. Lopez, R., Wang, R. & Seelig, G. A molecular multi-gene classifier for disease diagnostics. *Nat. Chem.* (2018).

34. Ke, Y., Ong, L. L., Shih, W. M. & Yin, P. Three-dimensional structures self-assembled from DNA bricks. *Science* (2012).
35. Rogers, W. B. & Manoharan, V. N. Programming colloidal phase transitions with DNA strand displacement. *Science* (2015).
36. Soloveichik, D., Seelig, G. & Winfree, E. DNA as a universal substrate for chemical kinetics. *Proc. Natl. Acad. Sci.* (2010).
37. Cardelli, L. Two-domain DNA strand displacement. in *Mathematical Structures in Computer Science* (2013).
38. Chen, Y. J. *et al.* Programmable chemical controllers made from DNA. *Nat. Nanotechnol.* (2013).
39. Srinivas, N., Parkin, J., Seelig, G., Winfree, E. & Soloveichik, D. Enzyme-free nucleic acid dynamical systems. *Science* (2017).
40. Dalchau, N., Seelig, G. & Phillips, A. in 84–99 (Springer, Cham, 2014).
41. Scalise, D. & Schulman, R. Designing modular reaction-diffusion programs for complex pattern formation. *Technology* **02,** 55–66 (2014).
42. Chirieleison, S. M., Allen, P. B., Simpson, Z. B., Ellington, A. D. & Chen, X. Pattern transformation with DNA circuits. *Nat Chem* **5,** 1000–1005 (2013).
43. Allen, P. B., Chen, X., Simpson, Z. B. & Ellington, A. D. Modeling scalable pattern generation in DNA reaction networks. *Nat. Comput.* (2014).
44. Rogers, W. B., Shih, W. M. & Manoharan, V. N. Using DNA to program the self-assembly of colloidal nanoparticles and microparticles. *Nature Reviews Materials* (2016).
45. Medintz, I. L., Uyeda, H. T., Goldman, E. R. & Mattoussi, H. Quantum dot bioconjugates for imaging, labelling and sensing. *Nat. Mater.* (2005).

5.7 Materials and methods

S1 Module design

A single ring module consists of a maximum of four components: Activator, Inhibitor, Threshold, and Reporter. It is known that an incoherent feedforward loop can produce a single pulse. However, we decided to design a *de novo* module to minimize the number of components required, since fewer components and reactions reduce chances of crosstalk and simplify both the sequence design and simulation processes. Our guideline for module design is as follows. First, the module should have a minimal number of components and exhibit pulse behavior. Second, DNA complexes should have similar lengths such that a common diffusion coefficient could be used for all complexes. Third, each complex should have a minimal number of functional domains to simplify parameter inference and spatial simulation *in silico*. Following this guideline, we designed a pulse-generator containing three components (Activator, Reporter, Inhibitor) and three functional domains (two toehold and one migration domains).

We designed two orthogonal modules for implementing concentric ring patterns. These modules have identical domain level designs but orthogonal sequences. Both modules use FAM fluorophore (excitation = 495 nm, emission = 520 nm) for signal reporting. For patterns involving two different colors, we also ordered Module 2 reporters functionalized with Cy5 (excitation = 648 nm, emission = 668 nm).

We performed sequence selection using the design utility in NUPACK, which provided sequences based on the desired domain level designs. Subsequently, we entered these sequences into the

analysis utility in NUPACK to validate that the sequences have minimal cross talk and obtained an estimate of rate constants based on the free energy differences in reactions ($\Delta\Delta G$).

One concern we had was that the forked toehold in the reporter might lead to leak between the reporter and the inhibitor complexes. However, in solution experiment show that such leakage is essentially nonexistent.

S2 Materials and methods

S1.1 DNA sequence design

All synthetic DNA gates used in this work have two functional domains: a single toehold domain and a single branch migration domain. We minimized the structural variations between gates to reduce simulation time and complexity. All toehold domains have 6 bp for optimal strand displacement speeds. All migration domains have 15 bp to optimize for sequence length and stability of the double strand complex.

S1.2 DNA gates preparation

Lyophilized synthetic DNA oligonucleotides purchased from IDT DNA were resuspended to 100 uM in 1X TAE Mg++ buffer and stored at -20^{o}C. Single strands like the activator and the threshold were diluted to ~ 10 uM before use.

Concentrations of DNA were measured using a NanoDrop. For non-functionalized single strand DNA, we entered the sequence into the "oligo" mode in the NanoDrop software.

For partially double stranded complexes like the reporter and the inhibitor, we anneal their respective top and bottoms strands in 1:1 ratio at 20 uM in PCR tubes for a final volume of 100 uL. We anneal the strands in a thermocycler by first heating them to 95^{o}C for 2 minutes, gradually cooling to 20^{o}C at a speed of -1^{o}C/min, and cooling for 10 minutes at 4 ^{o}C before finally retrieving them from the thermocycler. We dilute the annealed reporters and inhibitors in 1X TAE Mg++ to 4 uM and 10 uM, respectively, and store at room temperature in the dark until use.

S1.3 Spectrometry measurement

Kinetics measurements were performed using a spectrofluorometer (Horiba FluoroMax4). The spectrometer can accommodate up to 4 cuvettes (0.875 ml Fluorometer Micro Square Cells).

FAM fluorophores have excitation and emissions wavelengths at 495 nm and 520 nm, respectively. The spectrometer was set accordingly to detect FAM functionalized oligos. We set the shutter width to 3 nm and the integration time to 10 seconds, with 5 seconds in between each cuvette measurement. Prior to each experiment, the cuvettes were cleaned three times with 70% ethanol followed by nine washes with deionized water, one final ethanol wash, and air dried.

For each cuvette, 1X TAE Mg++ buffer and reporter gates were mixed for a reporter concentration of 20 nM and a final volume of 700 uL. Before triggering the reporters, we ran the spectrometer for 15 minutes to establish a baseline for the background fluorescence. The spectrometer was paused to add activator and inhibitor gates at the requisite concentrations. An external water bath was connected to the spectrometer for the full duration of the experiment to keep the samples at a constant temperature of 25^{o}C.

To normalize the spectrometry data, we measured the fluorescence of signal strands at concentrations of 10 nM, 20 nM, 30 nM, and 40 nM. We performed the same experiment on different days to ensure consistency and found minimal variation between measurements. We used this data to establish a standardized curve for converting fluorescence units to concentration (nM) and applied this conversion to all our spectrometry measurements.

S1.4 Making reaction chamber

We made a 3x3 grid on a large ¼'' thick clear acrylic sheet by cutting out nine 4.5 cm x 4.5 cm squares on the sheet using a laser cutter. We chose these dimensions to ensure that the assembled reactor chamber could fit into the gel imager. To make the reactor chambers, we placed the grid over another ¼'' thick clear acrylic sheet and taped the two sheets together on all four sides to create a leak-tight seal. We confirmed that the acrylic sheets are transparent when illuminated by light at the wavelengths of interest and did not interfere with the imaging of DNA-hydrogels.

To clean the reactor chambers after gel experiments, we first disassemble the grid and the underlying acrylic sheet by taking off the adhesives. After each gel experiment, we cleaned the grid and the sheet separately using liquid soap and warm water.

S1.5 Preparation of DNA-hydrogel sheets

To make 0.7% agarose gel, 0.35 g of low melting point agarose powder was added to 50 mL of 1X TAE Mg++ buffer in an Erlenmeyer flask and microwaved for 90 seconds or until the agarose had completely dissolved. Leftover hydrogel solution is stored at 37^{o}C with plastic wrap covering the flask to minimize evaporation.

The gel solution is cooled at room temperature to below 37^{o}C before synthetic DNA gates such as reporters and thresholds are added to prevent denaturing. After adding DNA complexes, we pipette 4 mL of DNA-hydrogel solution into a 5 mL Eppendorf tube and vortex on high for 10 seconds. Then the mixed solution is poured into a reaction chamber and chilled in a 4^{o}C fridge for 15 minutes. Once gelation occurs, we move the gel back to room temperature. Next, we puncture

circular cavities on the gel using the blunt end of a P10 pipette tip. We also made small 3D printed shapes as an alternative to using a pipette tip for creating cavities in the gel. The 3D printed parts include cylinders and X-shapes set at different intersecting angles. Each cavity can hold a volume of 40 uL.

S1.6 Gel imaging

We visualized the hydrogels using a Biorad PharosX gel imager. A 488 nm excitation laser and a 530 nm filter were used to image FAM fluorophores; a 637 nm excitation and a 695 nm filter were used to image Cy5 fluorophores. We scanned the images at 100 um resolution with the photomultiplier tube voltage at 80% of maximum. To make time course measurements, we installed a software (Mouse Recorder) that recorded specific mouse and keyboard actions to automatically take gel images at 30 minute intervals. Since gels dehydrate over time, we limited each gel experiment to less than 8 hours. When measuring gels containing both FAM and Cy5 fluorophores, we imaged the FAM channel first, then switched the filter and laser wavelength to the Cy5 channel.

S1.7 Gel image normalization

To create a calibration curve for converting gel imager fluorescence to concentration, we made six gels containing known concentrations of FAM functionalized signal strands (0 nM, 5 nM, 10 nM, 15 nM, 20 nM) and imaged these gels using the same imager settings as described in S1.6. We used ImageJ to calculate the average intensity in each gel, where we excluded the edges of the gels from intensity calculations because the gel is thicker there due to surface tension. We plotted the average fluorescence intensities against the known signal strand concentrations and fitted the data to obtain the equation for converting from fluorescence units to concentration (nM).

S1.8 Diffusion measurement

Because our oligos have the same length, we expect differences in diffusion rate to come from whether the DNA is single or double stranded. We used the diffusion coefficient of the signal strand as a proxy for other single strands in our system. For double strands, we use a modified reporter where the bottom strand is not functionalized with a quencher. We measured the diffusion coefficients of module M1 reporters and signal strand. For simplicity, we took the averaged value of the two diffusion coefficients and used it as the default value for all species in spatial modeling. To measure the diffusion coefficient, we pipetted 20 nM of either reporter or signal strand into a circular cavity punctured in a hydrogel made of 0.7% agarose only. The gel has the same dimensions as the other DNA-hydrogels. We took gel images periodically as the DNA strands diffuse over time.

Next, we used ImageJ to create a radial average intensity profile for each gel and normalize using the calibration curve from S1.7. For each intensity profile, we measured the position of the FWHM. Next, we plotted the positions against time and calculated fit to the plot using the 2D Einstein relation:

$$x^2 = 4Dt$$

, where x is the displacement (in our case, the position of the FWHM), D is the diffusion coefficient, and t is the time. The diffusion coefficients were later used in Visual DSD for spatial modeling.

The fitted diffusion coefficients are 5.6E-10 m^2/s for the reporter complex and 6.6E-10 m^2/s for the signal strand. These values are approximately five times greater than values for 20-bp DNA in free solution obtained from capillary electrophoretic measurements[53]. But because our strands

diffuse in 2D agarose gels, the results here may not necessarily be comparable due to differences in experiment setup.

S1.9 Gel image analysis and processing

We analyzed the gel images (saved as TIFF files) on ImageJ. First, we performed auto-leveling on the images to increase contrast. This step affected the appearance of the images but not the intensity measurements. Next, we set the length scale such that measurements are in centimeters. An open source plug-in was used to carry out radially averaged intensity measurements.

For gels containing both FAM and Cy5 fluorophores, we took images taken at the same time point from both channels and combined them into a composite. Because the gel imager takes greyscale images by default, we colored the composite images in post-processing to enhance visual contrast.

S3 Inferring reaction kinetics

S3.1 Chemical reaction network

We modeled the interactions between module components as the following set of bimolecular reactions:

$$Activator + Reporter \underset{k_{1r},\ k_{1f}}{\longleftrightarrow} Signal$$

$$Activator + Threshold \underset{k_{2r},\ k_{2f}}{\longleftrightarrow} Waste$$

$$Signal + Inhibitor \underset{k_{3r},\ k_{3f}}{\longleftrightarrow} Waste$$

S3.2 Strand displacement model

We constructed models of our DNA-based modules in Visual DSD, a compiler and programming language for describing DNA strand displacement reactions [cite]. The program is freely available at https://dsd.azurewebsites.net/beta/. We built the model to infer reaction rate constants using experimental data obtained from performing spectrometry on well-mixed solutions. First, we define the rate constants (k_{1f}, k_{1r}, k_{2f}, k_{2r}, k_{3f}, k_{3r}) and their range of possible values. For example:

k1f, (1.0e-7,2.0e-3)

Next, we define species in VDSD syntax, specifying the strands at the domain level:

```
def signal() = <t2^ d>                    (*nM^-1s^-1*)
def activator() = <t1^ d>
def reporter() = <t2^>{d1^*}[d]
def inhibitor() = {t2^*}[d]
```

, where the angled, curly, and square brackets denote top-, bottom-, and double-strand complexes, respectively.

We also specified leak rates and concentrations of potentially faulty DNA complexes (due to annealing or stoichiometric errors) and their range of values (in units of nM):

```
good_i,(0.0,1.0)
good_a,(0.0,1.0)
bad_r,(0.0,10.0)
leak_i, (1E-07, 0.002)
```

We parallel the structure of the VDSD program with corresponding in solution experiments. For experiments where we added in a DNA strand at a certain time point, we specified this condition with the following:

```
directive event activator() 1000.0*good_a @ T1
```

Here T1 denotes the time when activator was added. Parametrizing T1 is written as follows (units in seconds):

```
T1, (0.0,2000.0), 681.326827529902, real, random;
```

S3.3 Parameter inference

Using the model described in S2.1, we derived forward and reverse reaction rate constants for the four main reactions. We also fitted data for the full pulse-generator (reporter, inhibitor, activator, threshold). For the pulse-generator fits, we use rate constants derived from signal activation and inhibition spectrometry experiments as the initial values for parameter inference. The fit generates updated values of the activation and inhibition rate constants, which we use later in spatial simulations.

For each module, we tested all 5 reactions. We averaged the same reaction constant from different experiments. The result is used in simulating 2D spatial experiments.

S4 Reaction-diffusion spatial simulations

To simulate 2D patterns, we built spatial models using the CRN mode in Visual DSD. Compared to the DSD mode, the CRN mode abstracts the interactions between module components as chemical reactions equations, without detailing the compositions of the reactants. We chose this simplified approach because it vastly reduces simulation time without compromising on simulation accuracy.

To construct the model, we specify the initial and boundary conditions using the syntax of Visual DSD. First, we define reaction rate constants using values inferred from spectrometry data (See Supplementary Table 3), where rate constants are expressed:

```
directive parameters [k1f = 1e-4; k1r = 1e-5; k2f = 5e-5; k2r = 1e-6]        (*nM^-1s^-1*)
```

Next, we define the spatiotemporal mesh and step sizes:

```
directive nx 101            (*step size, unitless*)
directive xmax 0.045        (*in meters*)
```

We define a common diffusion coefficient (2E-9 m^2/s) for all strands since differences between strand sizes are negligible:

```
directive defaultdiffusion 6e-10
```

We use the following code to define the positions of cavities and the concentrations of initiating strands contained in the cavities:

```
directive spatialic centralcore {width=0.1; species = Act1; inner=2000.0}
```

Here, the first term in the curly bracket specifies the size of the cavity, defined in units of … The second term specifies the reactant in the cavity. The third term specifies the concentration of the reactant in units of nM.

Next, we describe the reactions and specify the appropriate rate constant:

```
Act1 + Rep1 ->{r2} S1 + W1 |
 Inh1 + S1 ->{r2} W2 |
```

The two equations above describe the activation and inhibition of signals, respectively. Finally, we list the molecule type and their initial concentrations in the gel:

```
init Act1 2000 |
init Inh1 N*600 |
init Rep1
```

Supplementary Figures

$$Activator + Reporter \underset{k_{1r},\ k_{1f}}{\longleftrightarrow} Signal$$

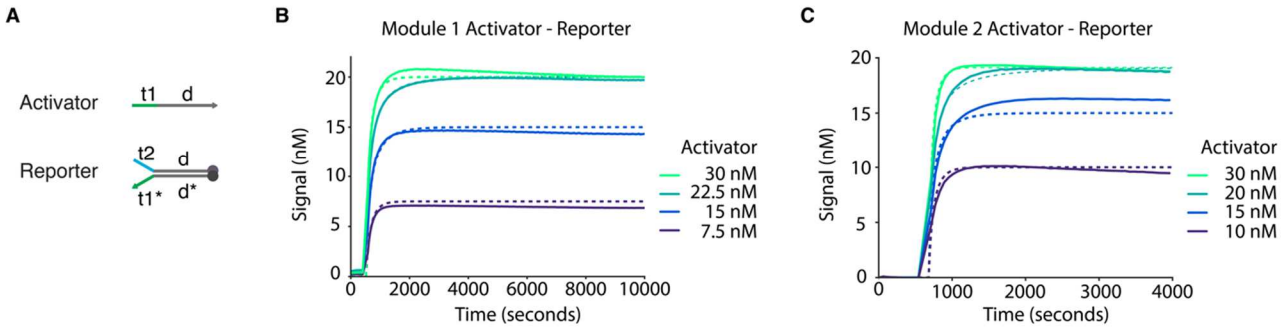

*Supplementary Figure 1: reaction kinetics for reporter activation***.** We added 20 nM of reporter first to establish a baseline of background florescence. Then we paused the spectrometer to add to the indicated concentrations of activators. Solid lines show experimental data; dashed lines show simulated fits.

$$Signal + Inhibitor \underset{k_{3r},\ k_{3f}}{\longleftrightarrow} Waste$$

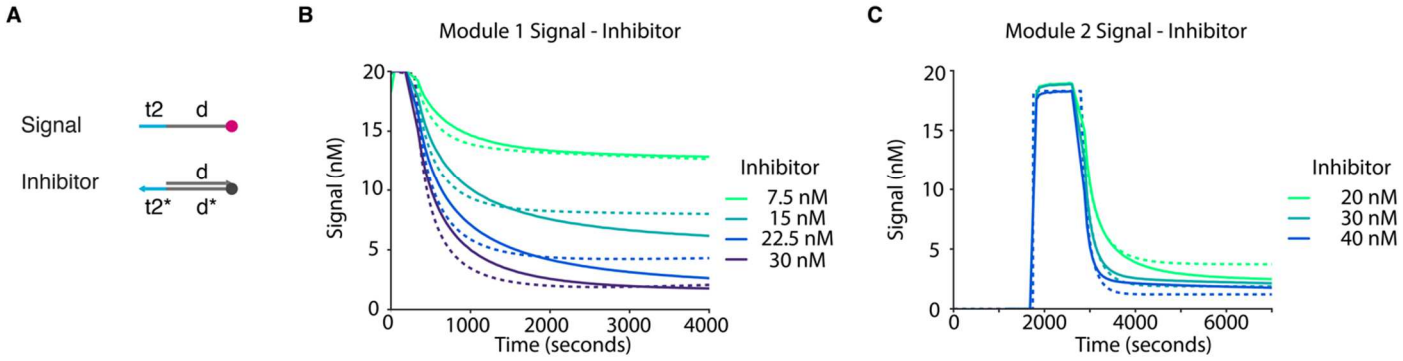

Supplementary Figure 2: reaction kinetics for signal inhibition. 20 nM of reporter was added to the buffer solution first, which was activated by 40 nM of activator. Finally, we added inhibitor at the indicated concentrations.

$$Activator + Reporter \underset{k_{1r},\ k_{1f}}{\longleftrightarrow} Signal$$

$$Signal + Inhibitor \underset{k_{3r},\ k_{3f}}{\longleftrightarrow} Waste$$

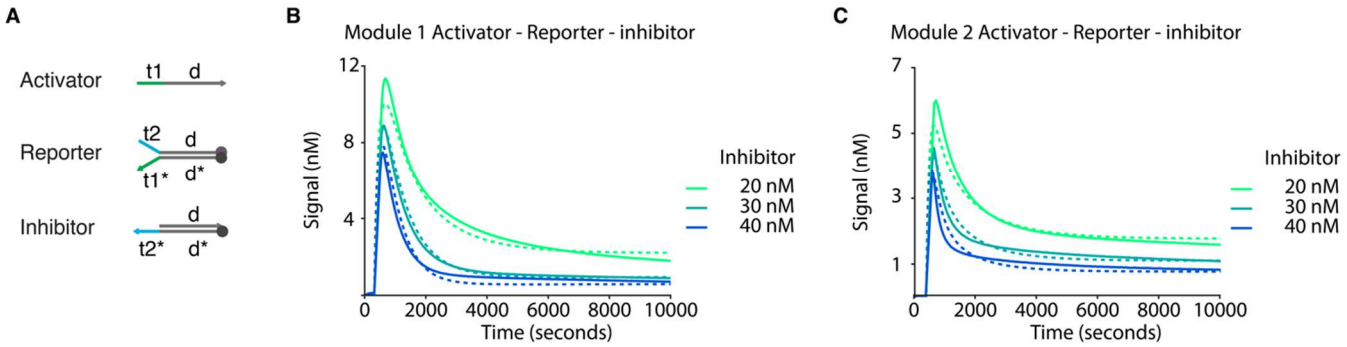

Supplementary Figure 3: reaction kinetics of pulse response. 40 nM of activator was added to each sample solution containing 20 nM of reporter and inhibitor at the indicated level of concentration.

$$Activator + Reporter \underset{k_{1r},\ k_{1f}}{\longleftrightarrow} Signal$$

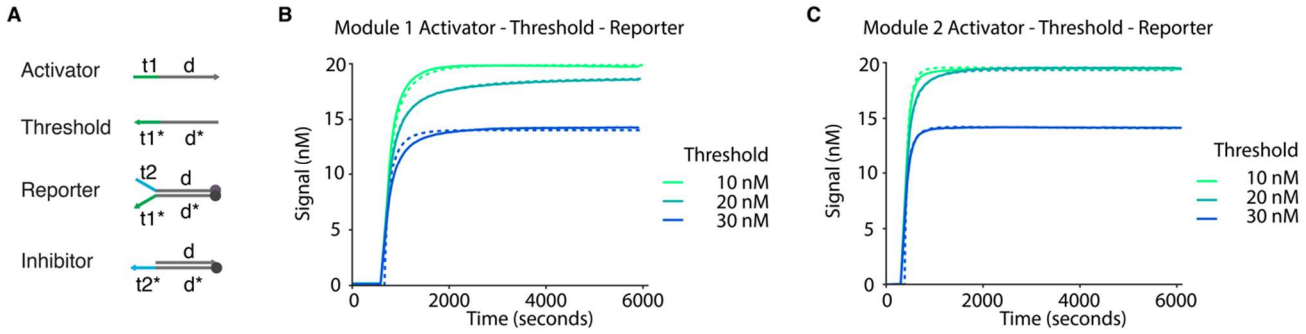

Supplementary Figure 4: reaction kinetics of adding threshold to reporter activation. 40 nM of activators were added to each sample solution containing 20 nM of reporter and threshold at the indicated concentrations.

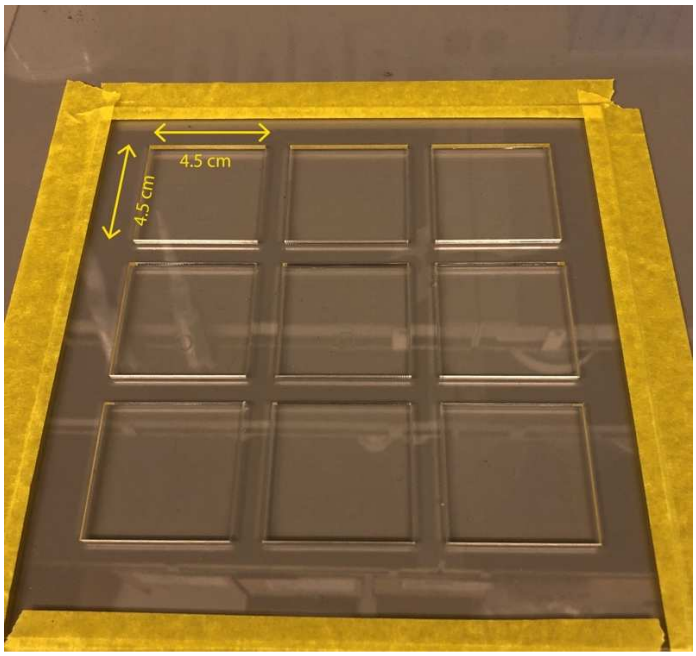

Supplementary Figure 5: acrylic reactor chamber setup. To make the reaction chamber, we taped two customized acrylic pieces together. The top piece contains nine grids measuring 4.5 cm x 4.5 cm. The bottom piece is a flat sheet of acrylic. Both sheets measure 0.25'' in thickness.

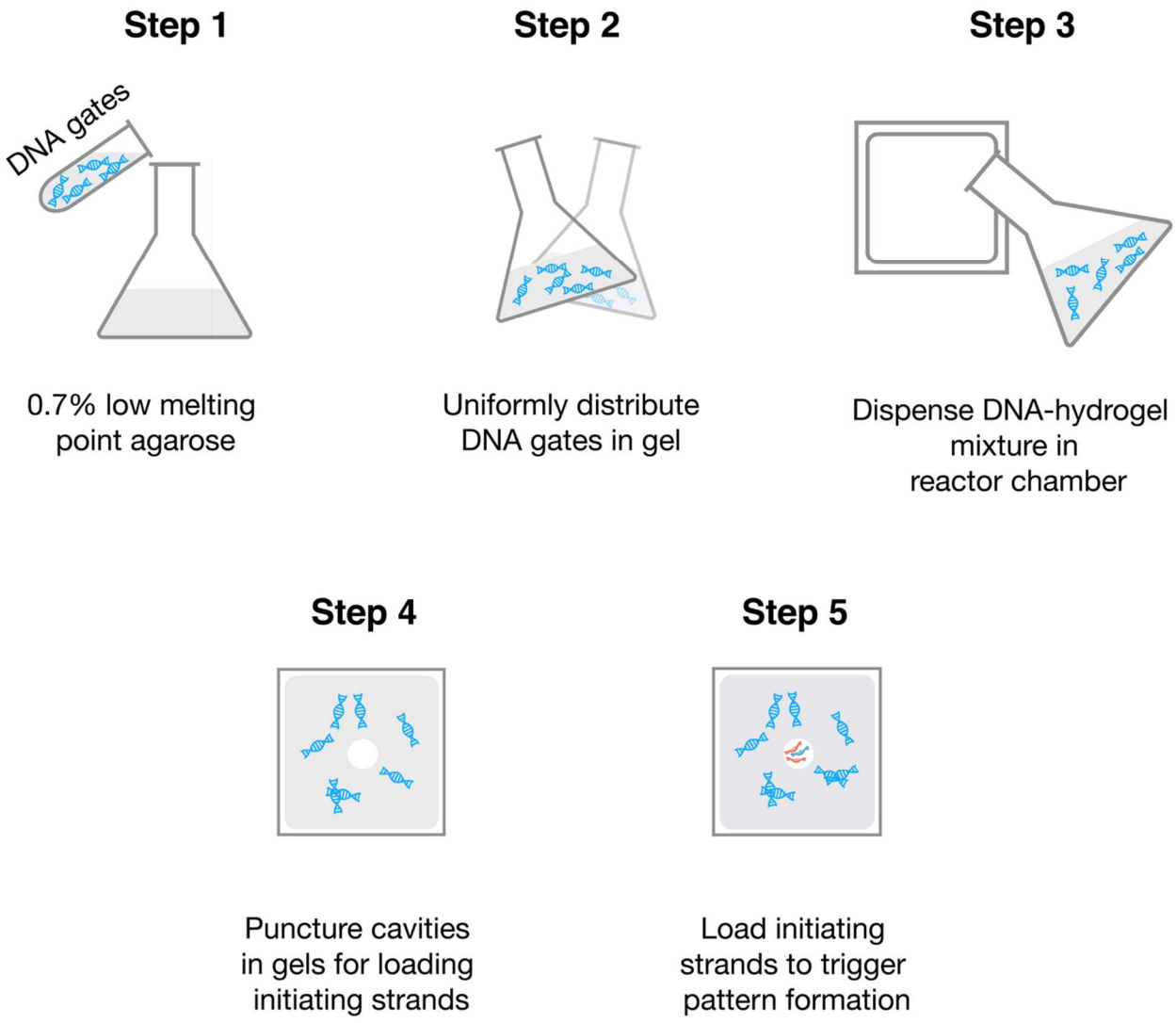

Supplementary Figure 6: workflow for synthesizing DNA-hydrogels. We used low melting point agarose to minimize denaturing of DNA complexes. After thoroughly mixing DNA with agarose gel solution, we dispense the mixture in acrylic reactor chambers. To make non-circular cavities, we placed 3D printed shapes in the hydrogel solution before gelation. To make circular cavities, we punctured directly on the hydrogel (post-gelation) using the blunt end of a 10 uL pipette tip. We pipetted initiator strands like activators and inhibitors into the cavities to trigger pattern formation. Each cavity can hold a maximum of 40 uL.

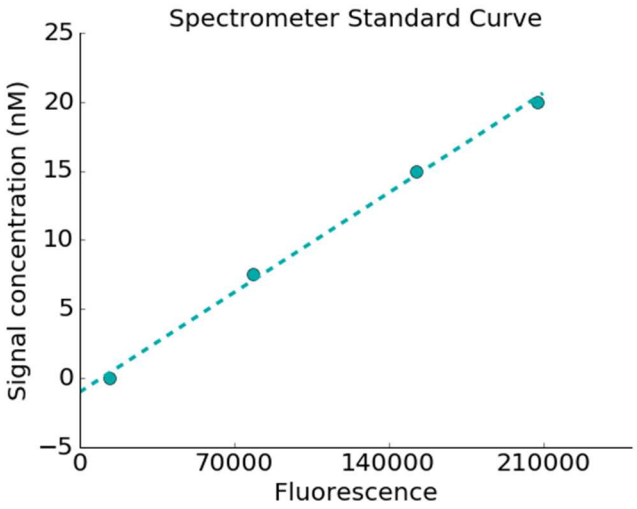

Supplementary Figure 7: calibration curve for spectrometer. Standard curve derived from measuring signal strand at four concentrations in a well-mixed solution. We convert fluorescence units to nM before performing inference on the data.

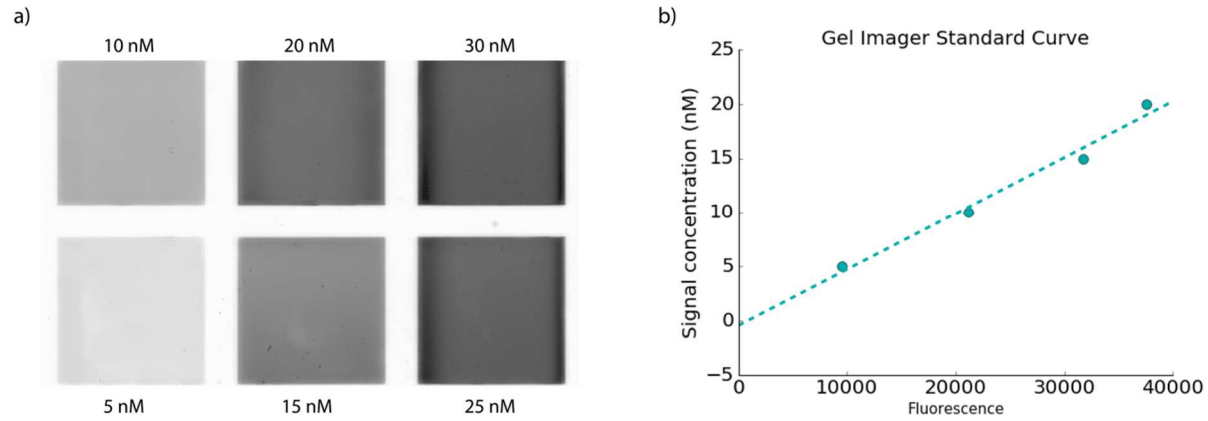

Supplementary Figure 8: calibration curve for gel imager. a) Gels uniformly embedded with the labeled concentrations of signal strands. b) Calibration curve for converting gel imager fluorescence intensity to signal strand concentrations.

	D (cm^2/hr)	D (m^2/s)
Module 1 reporter complex	0.020	5.6E-10
Module 1 signal strand	0.024	6.6E-10

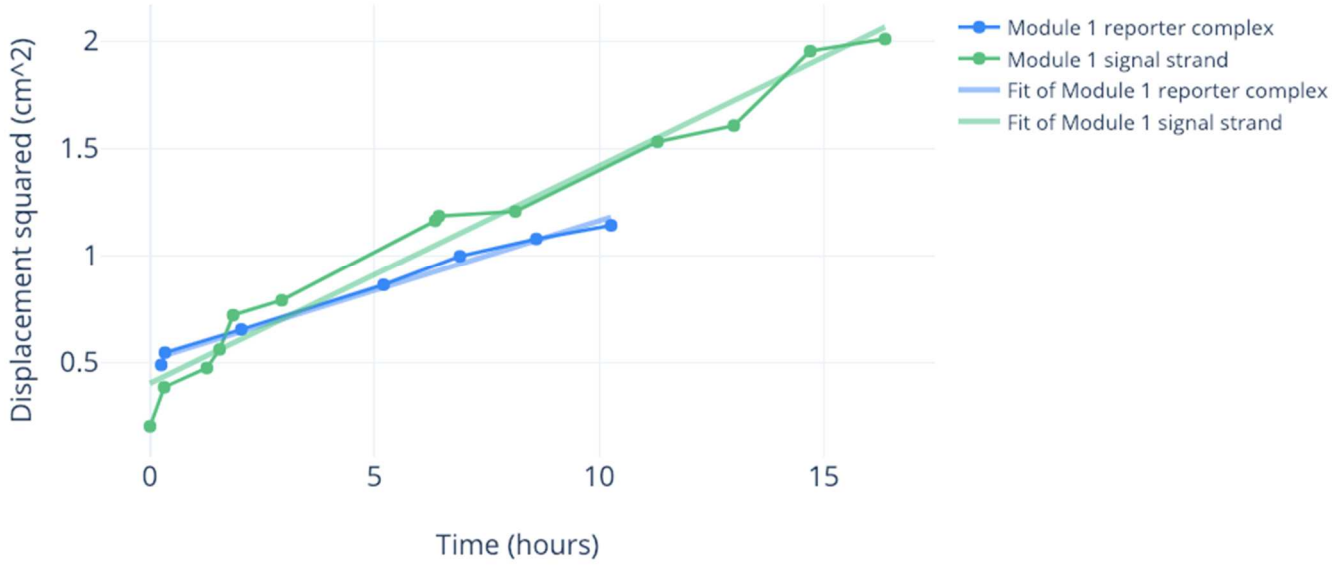

Supplementary Figure 9: diffusion coefficients of signal strand and reporter. For obtain each data point on the plot, we first measured the position of the FWHM on a radially averaged intensity profile at the specified time point, then calculated the square of this position. We plotted displacement squared against time and fitted the data to the 2D mean square displacement equation. The table at the top shows the diffusion coefficients for the signal strand and the report complex in units of cm^2/hr and m^2/s.

a) Experiment setup

Cavity:
Activator (as indicated)
Inhibitor (200 nM)

Gel:
Threshold (as indicated)
Reporter (20 nM)

b)

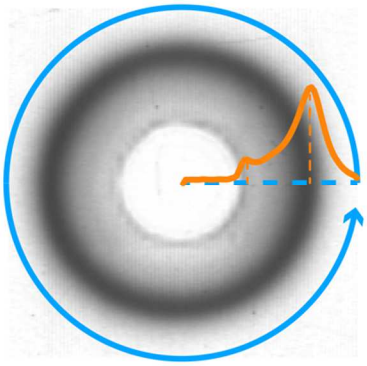

Supplementary Figure 10: experiment setup of single ring patterns in threshold-added gels. **a)** The concentrations of reactants and where they were added. Values of activator and threshold concentrations can be found in **Supplementary Fig. 12**. **b)** An example showing how we measured the radially averaged intensity profile using gel images. Two visible "peaks" are visible in each profile. The smaller peak corresponds to the edge of the cavity. The larger peak corresponds to signal pulse.

a) Simulation setup

```
Activator + Reporter -> {r1f} Signal + W1
Signal + W1  -> {r1r} Activator + Reporter

Inhibitor + Signal ->{r3f} W2
W2 ->{r3r} Inhibitor + Signal

Activator + Threshold ->{r2f} W3
W3 ->{r2r} Activator + Threshold
```

b) Simulation parameters (from experiments)

```
r1f = 1.75e-4   nM-1S-1
r1r = 9e-5      nM-1S-1
r3f = 1.3e-4    nM-1S-1
r3r = 4.25e-5   nM-1S-1
r2f = 1e-3      nM-1S-1
r2r = 1e-7      nM-1S-1

D = 6e-10       m^2/s
```

Supplementary Figure 11: simulation setup for single ring pattern in threshold-added gels. **a)** The chemical reactions for performing spatial simulations of single ring patterns in Visual DSD. The simulation includes the forward and reverse rate constants. **b)** The rate constants and diffusion coefficient used in the simulation. We derived these parameters from experiments.

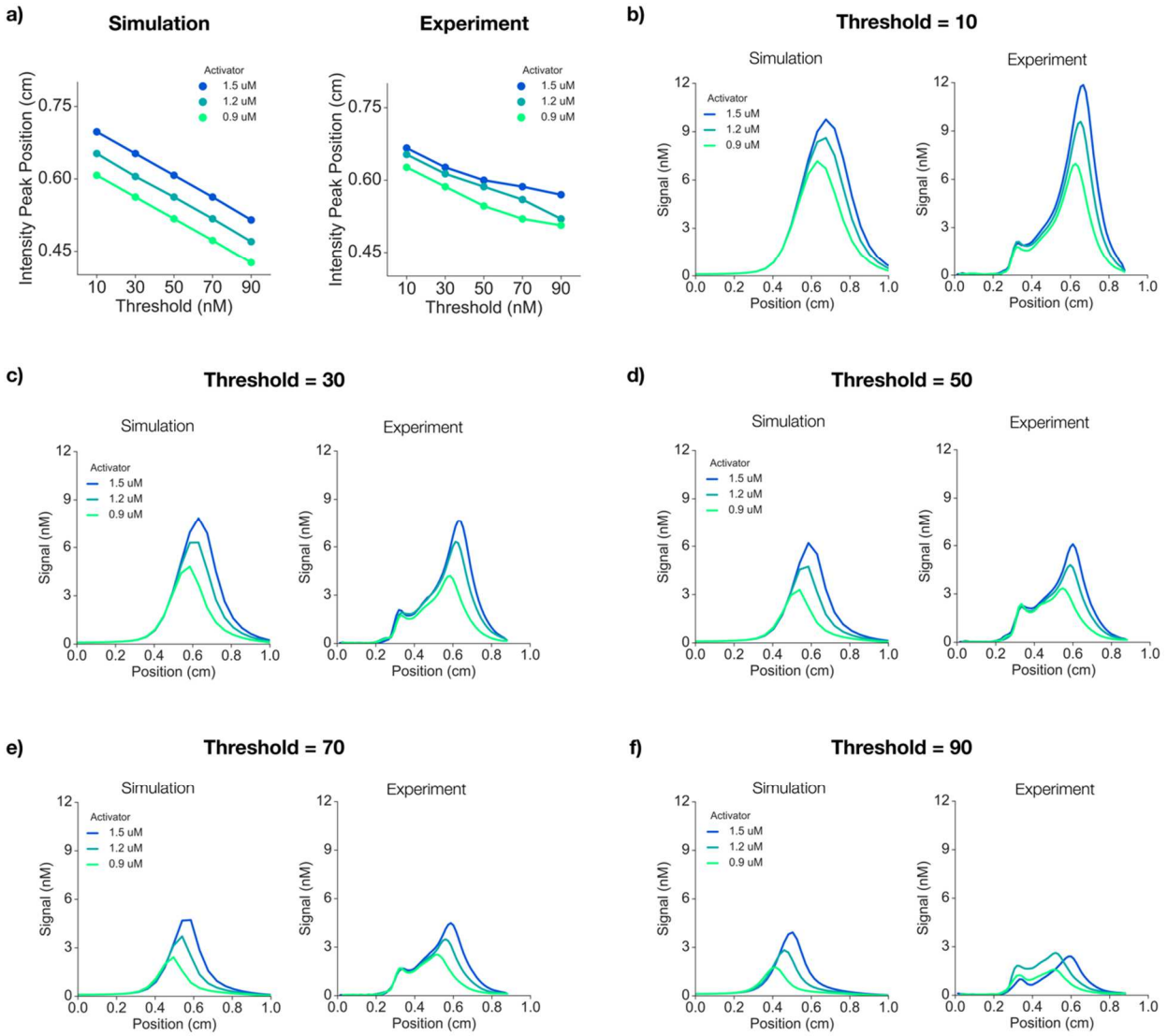

Supplementary Figure 12: single ring patterns in threshold-added gels (in vitro vs in silico). **a)** The threshold is more effective than the activator for changing the positions of intensity peaks, a proxy for ring radius. Each point on the plot represents the peak intensity position of a ring pattern, as measured from the corresponding radially averaged intensity profiles. **b)-f)** Comparisons between the radially averaged intensity profiles of simulated and experimentally realized ring patterns for the setups described in **Supplementary Figs. 10** and **11**.

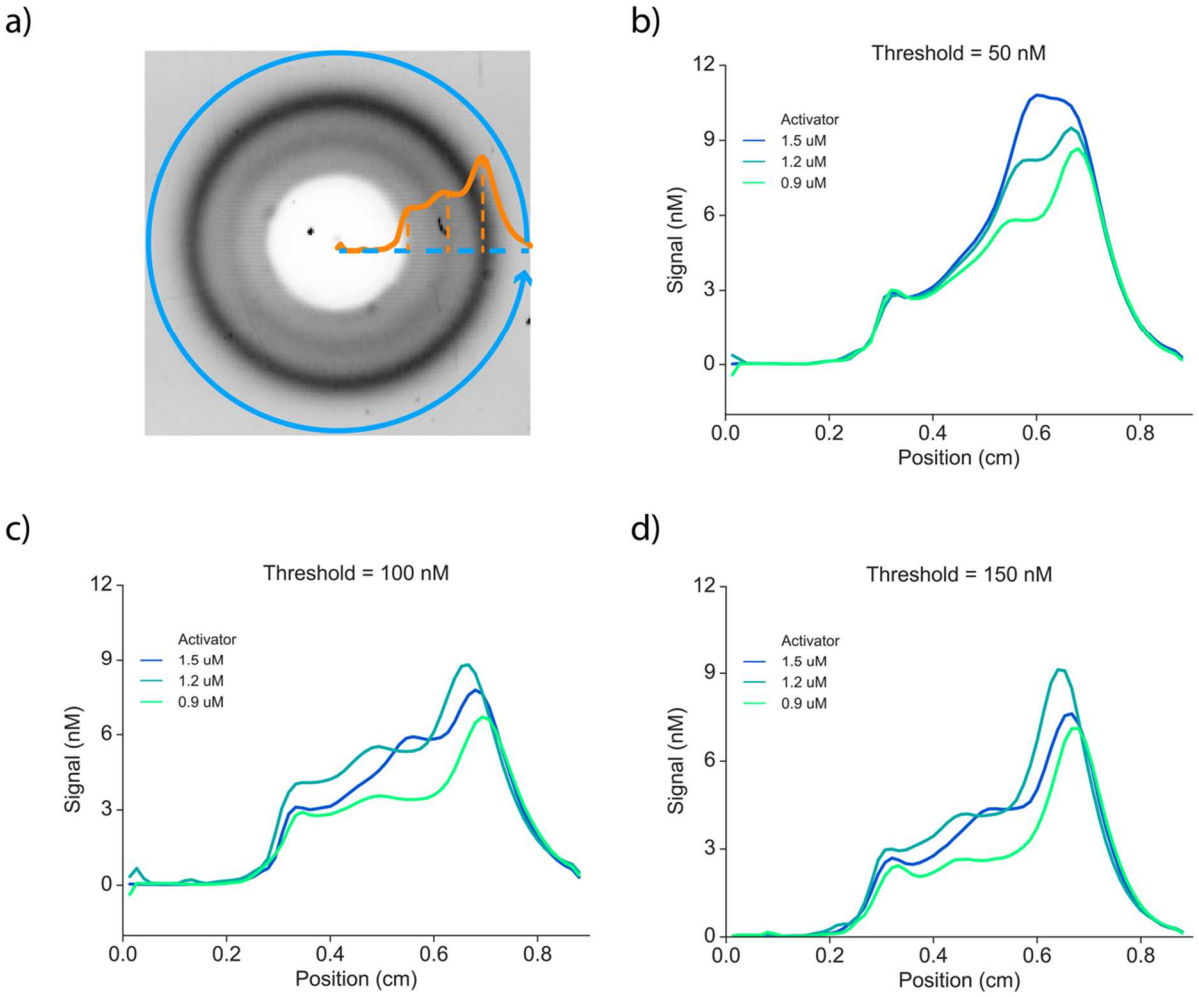

Supplementary Figure 13: intensity profiles for concentric ring patterns. **a)** Three visible "peaks" are visible in each profile. The smallest peak corresponds to the edge of the cavity. A second peak indicates the inner ring. The largest peak corresponds to the outer ring. **b)-d)** Each plot shows the intensity profiles from three gels embedded with the indicated concentration of threshold, but triggered with three different activator concentrations. For the inner ring intensity peaks, we measured the position where the signal showed the greatest inflection. The positions of intensity peaks and their dependence on threshold and activator
concentrations are shown in **Fig. 3G**.

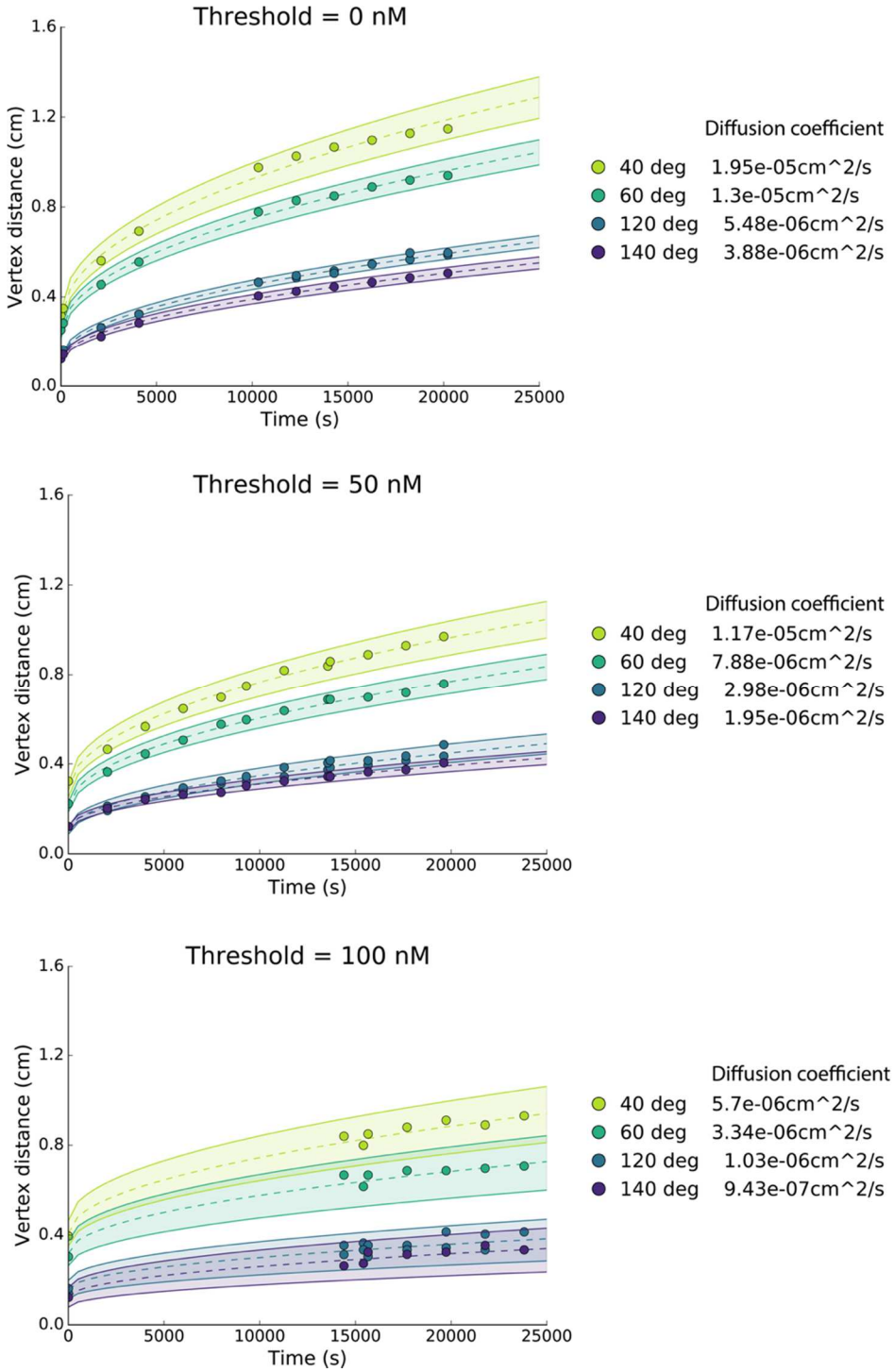

Supplementary Figure 14: angular and threshold on effective diffusion. The effective diffusion coefficient incorporates the reaction and diffusion aspects of the propagating signal. Each data point corresponds to the position of peak intensity relative to the center of the cavity. We fitted each dataset to the 2D Einstein equation to obtain the effective diffusion coefficient. For the last plot, the missing time points were due to malfunctions in the gel image.

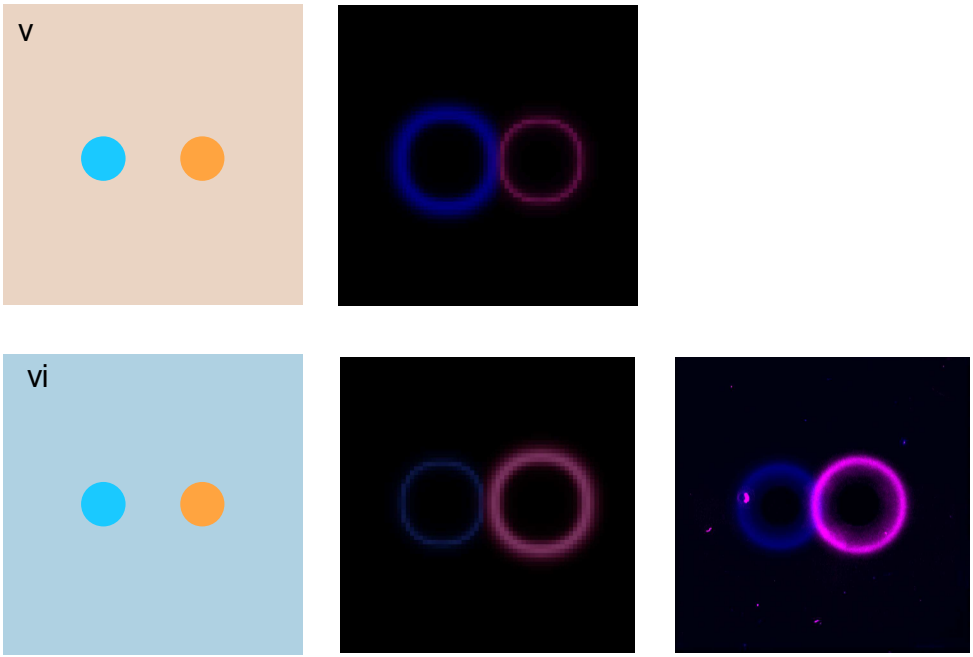

Supplementary Figure 15: two colored rings subjected to different threshold levels. Each gel was embedded with components from modules M1 and M2, which are orthogonal in sequence and have different reporter fluorophores. M1 reporters have FAM fluorophores (in magenta); M2 reporters have Cy5 fluorophores (in blue). The left column shows the gel setup; the center column shows simulation results; the right column shows gel image results. The top row and bottom rows show gels embedded with M1 and M2 threshold, respectively. For each gel, we pipetted M1 initiators in the left cavity and M2 initiators in the right cavity (activator = 2000 nM, inhibitor = 400 nM).

Supplementary Tables

Supplementary Table 1

Strand name	Sequence
AITR4.A	AAC CCA CAA AAC AAA ACC TCC
AITR4.T	GGA GGT TTT GTT TTG TGG GTT
AITR4.Rtop	CTT ATA CAA AAC AAA ACC TCC /36-FAM/
AITR4.Rbot	/5IABkFQ/GGA GGT TTT GTT TTG TGG GTT
AITR4.Itop	CAA AAC AAA ACC TCC
AITR4.Ibot	/5IABkFQ/GGA GGT TTT GTT TTG TAT AAG
AITR5.A	CTT CTC CAT TCC TAC ATT TCC
AITR5.T	GGA AAT GTA GGA ATG GAG AAG
AITR5.Rtop.FAM	CAA TAT CAT TCC TAC ATT TCC/36-FAM/
AITR5.Rbot.FAM	/5IABkFQ/GGA AAT GTA GGA ATG GAG AAG
AITR5.Rtop.Cy5	CAA TAT CAT TCC TAC ATT TCC /3Cy5Sp/
AITR5.Itop.	CAT TCC TAC ATT TCC
AITR5.Ibot.FAM	/5IABkFQ/GGA AAT GTA GGA ATG ATA TTG
AITR5.Ibot.Cy5	/5IAbRQ/GGA AAT GTA GGA ATG ATA TTG

Supplementary Table 2: rate constants obtained by fitting Visual DSD strand displacement model to spectrometry data. For rate constants that appear in multiple reactions, we provide the averaged value and the standard deviation.

Rate constant (Module 1)	signal activation	Signal inhibition	signal activation and inhibition	signal activation with threshold	Average	Stdev
k1f	3.65E-04		1.61E-04		1.75E-04	1.83E-04
k1r	1.96E-04		4.90E-05		9.38E-05	8.88E-05
k3f		1.91E-04	7.13E-05		1.31E-04	
k3r		2.51E-05	5.99E-05		4.25E-05	
Rate constant (Module 2)	signal activation	signal inhibition	signal activation with threshold	signal activation and inhibition	Average	Stdev
k1f	9.63E-04		7.03E-04	1.35E-04	6.00E-04	4.23E-04
k1r	2.02E-04		1.72E-06	4.02E-04	2.02E-04	2.00E-04
k2f			1.96E-03		1.96E-03	
k2r			1.06E-07		1.06E-07	
k3f		1.92E-04		1.32E-04	1.62E-04	4.24E-05
k3r		1.68E-05		1.23E-05	1.46E-05	3.18E-06

Supplementary Table 3: detailed experiment setups for DNA-hydrogels

Single ring experiment (Figure 2G)	
Gel	20 nM reporter (M1)
Cavity	Activator (M1); Inhibitor (M1)

Threshold experiment (Figure 3C)	
Gel	20 nM reporter (M2); Threshold (M2)
Cavity	Activator (M2); Inhibitor (M2)

Two concentric ring experiment (Figure 3F)	
Gel	20 nM reporter (M1); 20 nM reporter (M2); Threshold (M2)
Cavity	Activator (M1); Inhibitor (M1); Activator (M2); Inhibitor (M2)

Two color experiments (Figure 3H, i&ii)	
Gel	20 nM reporter (M1); 20 nM reporter (Cy5, M2); Threshold (M2)
Cavity	Activator (M1); Inhibitor (M1); Activator (M2); Inhibitor (M2)

Two color experiments (Figure 3H, iii&iv)	
Gel	20 nM reporter (M1); 20 nM reporter (Cy5, M2); Threshold (M2)
Cavity	Activator (M1); Inhibitor (M1); Activator (M2); Inhibitor (M2)

Non-isotropic cavity experiments	
Gel	20 nM reporter (M1)
Cavity	Activator (M1)

Non-isotropic cavity experiments	
Gel	20 nM reporter (M1); Threshold (M1)
Cavity	Activator (M1)

Interference pattern experiments	
Gel	20 nM reporter (M1); Threshold (M1)
Cavity	Activator (M1)

Supplementary Videos

Supplementary video 1 Time course of single ring pattern for different activator and inhibitor concentration ratios as acquired over 5 hours (Fig. 2G).

Supplementary video 2 Time course of concentric ring patterns for different activator concentrations with embedded threshold concentrations of 50 nM (Fig. 3F).

Supplementary video 3 Time course of concentric ring patterns for different activator concentrations with embedded threshold concentrations of 100 nM (Fig. 3F).

Supplementary video 4 Evolution of patterns corresponding to Fig. 4D first row.

Supplementary video 5 Evolution of patterns corresponding Fig. 4D second row.

Supplementary video 6 Evolution of patterns corresponding to Fig. 4D third row.

Supplementary video 7 Evolution of patterns corresponding to Fig. 4D fourth row.

Supplementary video 8 Evolution of patterns corresponding to Supplementary Fig. 15 (gel V).

Supplementary video 9 Evolution of patterns corresponding to Supplementary Fig. 15 (gel VI).